EXCERPT FROM:

Damping characteristics of combustion chambers coupled with acoustic elements

Zoltán Faragó
Sebastian Markgraf

DLR – LA – HF – RP – 020
DLR
Deutsches Zentrum für Luft- und Raumfahrt

R&T Program
CNES / CNRS / ONERA / DLR / EADS ST / SNECMA
"*High Frequency Combustion Instabilities*"

Lampoldshausen, 2006-03-22

Zoltán Faragó
German Aerospace Research Center (DLR)
D 74239 Hardthausen
Zoltan.Farago@dlr.de

Damping characteristics of combustion chambers coupled with acoustic elements

Sebastian Markgraf

Internship report
01. September 2005 to 31. January 2006

Supervisor
Zoltán Faragó

A. Abstract

This work deals with the influence of damping elements on the acoustically excited pressure oscillations in a laboratory scale combustion chamber and a steam generator coupled with up to 42 resonator tubes. The main task is to point out, how damping in a combustion chamber works and how it can be influenced. The effects of different chamber setups are pointed out and several excitation methods are investigated.

The text focuses on effects that cannot be explained by the theory of linear acoustics. The phenomenon of mode-to-mode conversion, i.e. the energy transfer between modes is described for combustion chambers coupled with acoustic elements and the existence of a hierarchy of acoustical modes in cylindrical chambers is shown. The hierarchy describes the interaction of modes of lower and higher frequency in reference to the damping.

B. Acknowledgment

First and foremost I have to thank my supervisor Mr. Zoltán Faragó for his patience and willingness to answer even the most trivial questions. His colorful explanations were always of great help to understand difficult tasks. Furthermore I have to appreciate his helpfulness not only during problems at work but also during leisure time.

Also I have to thank the team of the propulsion institute for their courteousness and the theoretical background they offered to me.

Table of contents

The French German coop research and technology program "High frequency combustion instabilities" engages in the investigation of the oscillations in combustion chambers caused by acoustic excitations. The evolved pressure fluctuations can lead to problems like increased noise and unsteady combustion behavior, but can also cause structural damages through excessive oscillations or even the destruction of the engines. Other effects are variations in thrust vector, oscillatory propellant flow rates and high heat transfer rates. Participants in the program are also CNES, CNRS, EADS and SNECMA.

For the experiments several common research chambers (CRC) are used whereas two of them are located in Lampoldshausen. One of them is examined by Bernhard Knapp [1] under real combustion conditions. The other one is used by several editors under the supervision of Zoltán Faragó [2]…[6] for tests at room temperature and without injection and spraying.

First measurements were done by Eunan J. McEniry [3]. The quintessence of these tests was the good comparability of different excitation methods. It was shown that the acoustical excitation by the use of a loudspeaker and therefore the placement of another damping element doesn't affect the acoustical properties compared to the mechanical hammer excitation.

Alexander N. Uryu's [4] works showed the coherency between the measured full width at half maximum of acoustic modes and the pedestal intensity of the peaks and pointed out the systematic errors caused by the gauging of the 3 dB width of weak modes.

The report of Thibaut A. Barbotin [5] is focused on the feature of mode-to-mode conversion in a CRC coupled with one resonator and the influence of resonator shape and length on damping and energy content of the acoustic field.

Finally Guillaume Dellea's [6] task was to broaden the field of application from a one-dimensional CRC to a steam generator (SG) where the influence of the length was not negligible and the extension of the number of resonators up to 42.

After the introduction to the basic theory of acoustics, the measurement principles and the design of the test bench, this study deals with the influence of various numbers of damping elements on the pressure oscillations in a steam generator (SG). During the work different methods for exciting the acoustical modes are examined. The main task is to point out how damping in the chamber works and how it can be biased. Former measurements are approved and non-linear effects like mode-to-mode conversion are investigated. The number of resonators attached to the chamber is changed from zero to 42 and their length is altered from zero to 105 mm. The length and shape of the chamber itself is varied from 44 mm and cylindrical shape to 684 mm with exit nozzle.

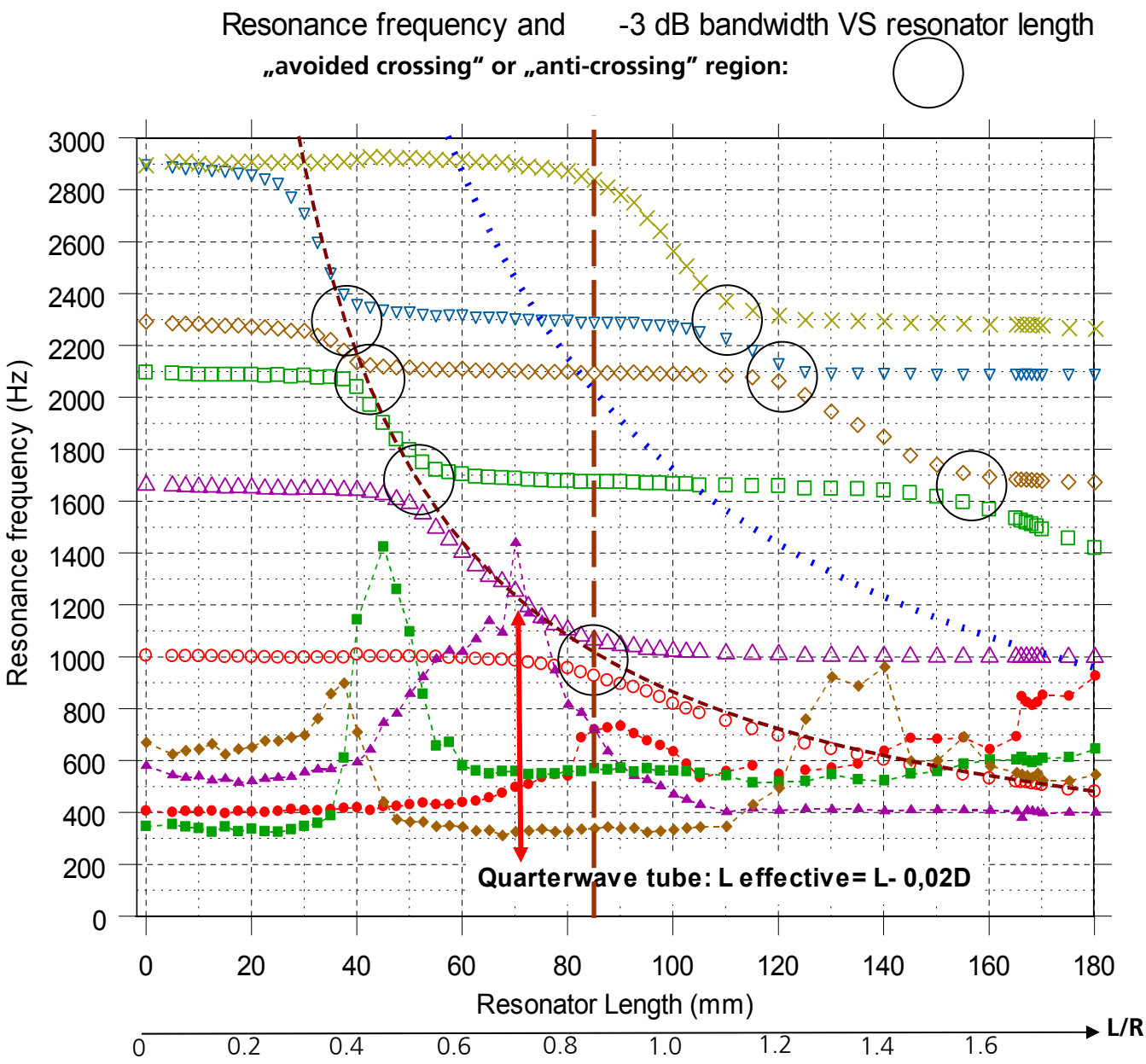

Figure 1.5.2: Frequency and FWHM of acoustical eigenmodes in system of CRC coupled with resonator cavity, CRC radius 100 mm [5]
circle = 1T, triangle = 2T, quad = 1R, diamond = 3T (empty = frequency, solid = FWHM)

$$l \cdot \frac{c}{2L} = \frac{\alpha_{n,m} \cdot c}{2 \cdot \pi \cdot R} \qquad (14)$$

$$\frac{(2 \cdot l - 1) \cdot c}{4 \cdot L} = \frac{\alpha_{n,m} \cdot c}{2 \cdot \pi \cdot R} \qquad (15)$$

Crossing for resonance frequency between experiment and λ/2-hypebolas appears if equation (14) is fulfilled. Anti-crossing between experiment and λ/4-hypebolas appears if equation (15) is fulfilled. In this the λ/4-hypebolas (solid hyperbolas in figure 1.5.3) do cross the cylindrical transverse modes.

The "avoided crossing" or "anti-crossing" in figure 1.5.2 can be explained in the following way: If equation (15) is true, both requirements should be fulfilled: 1) The quarter wave tube should show a velocity profile as presented in figure 1.2.1, and 2) the pressure distribution in the cylindrical chamber should be like in figure 1.1.1. These pressure and velocity distributions, however, suspend each other.

A crossing point between a radial mode and the λ/4-osciallation of the coupled resonator cannot be realized because the λ/4-oscillataion requires a pressure node at the resonator inlet, and, at the same time and at the same location, the radial cylindrical mode requires a pressure anti-node at the radial position r/R = 1 in the cylindrical chamber.

Similarly, a crossing point between a tangential mode and the λ/4-oscillation of the coupled resonator cannot be realized either because the λ/4-oscillation requires a radial velocity fluctuation at the orifice of the resonator, but the tangential eigenmode requires an azimuthal oscillation at the same location.

In the anti-crossing regions in figure 1.5.2 we can find two eigenmodes close to each other. The one of them has a slightly higher and the other one a slightly lower frequency than that of the belonging parental chamber modes. Denoting the avoided crossing regions according the denotation of the parental modes, the two eigenmodes are called + (plus) and – (minus) mode. An example can be found in figure 1.5.2 around the resonator length region of $\approx 0.8 < L/R < \approx 0.9$ in the frequency range of $\approx 900 < f < \approx 1100$ Hz for the 1T mode. The lower mode (red circles) is named **1T- mode** and the upper one (violet triangle) **1T+ mode**. Both show similarities to the 1T mode, however, the **1T-** has a pressure node inside the resonator and the **1T+** a pressure node in the chamber in front of the resonator.

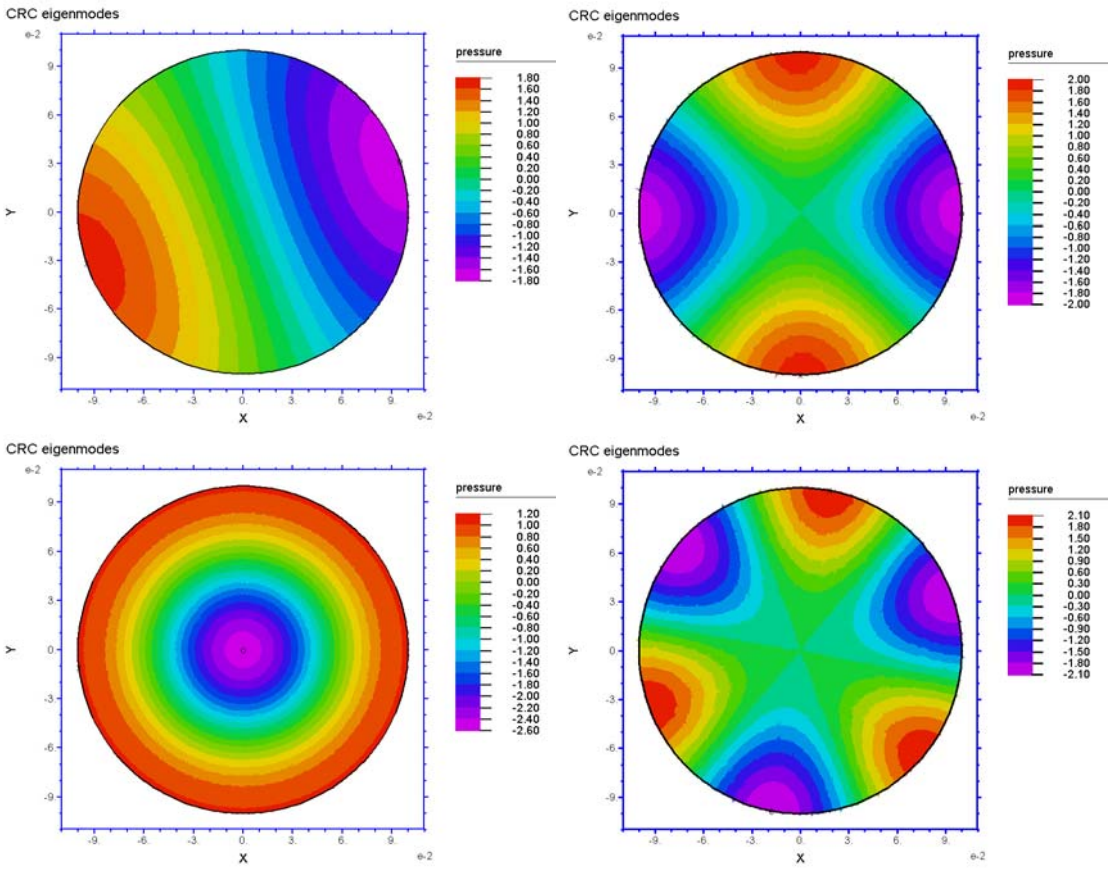

Figure 1.1.1: Pressure distribution in the chamber
for the acoustical modes 1T, 2T (top), 1R and 3T (bottom) [8]

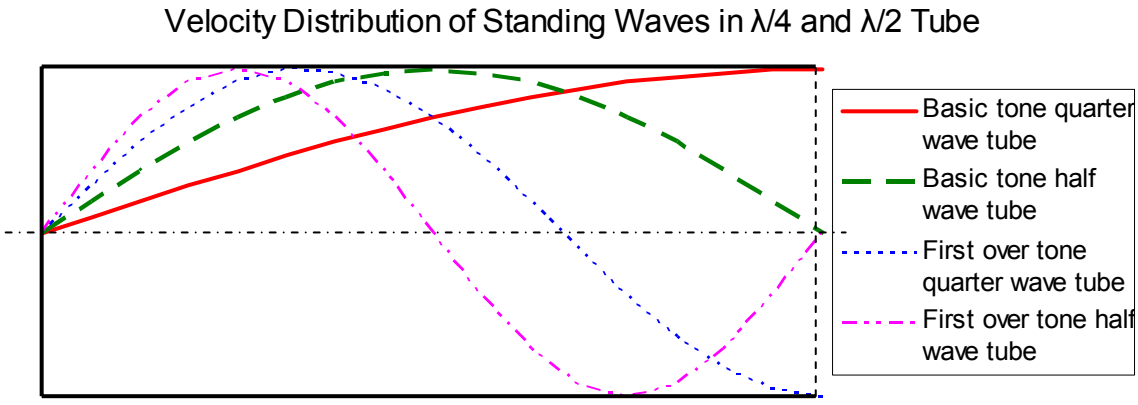

Figure 1.2.1: Velocity distribution in lambda-quarter and lambda-half tubes

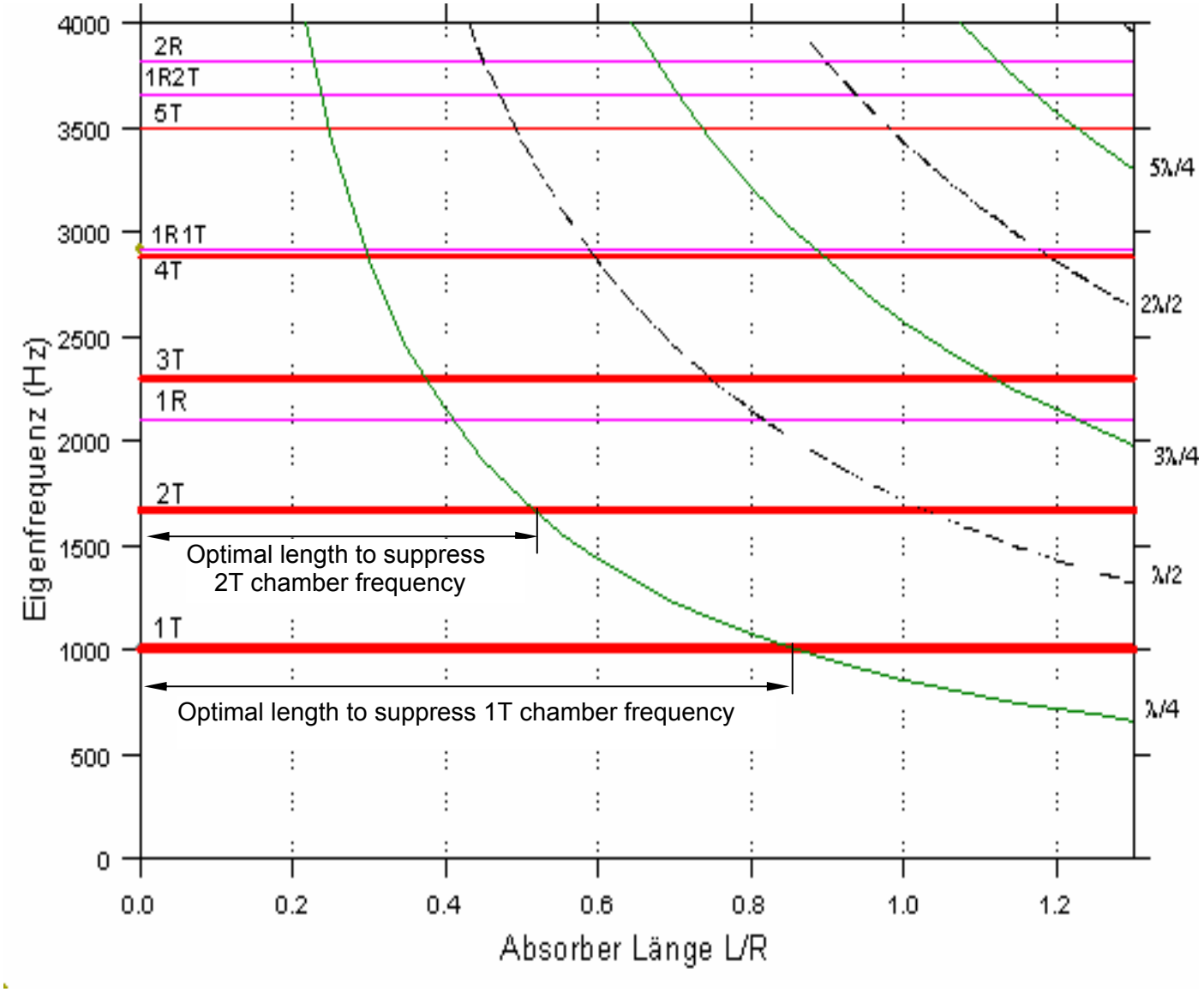

Figure 1.5.3: Fundamental chamber frequencies and cavity eigenfrequencies

$$f_l = l \cdot \frac{c}{2L}$$ Resonance frequency for λ/2-hypebolas

$$f_l = \frac{(2 \cdot l - 1) \cdot c}{4 \cdot L}$$ Resonance frequency for λ/4 hyperbolas

$$f_{m,n} = \frac{\alpha_{n,m} \cdot c}{2 \cdot \pi \cdot R}$$ Resonance frequency for cylindrical chamber modes

For $\alpha_{n,m}$ values see table 3.1.1

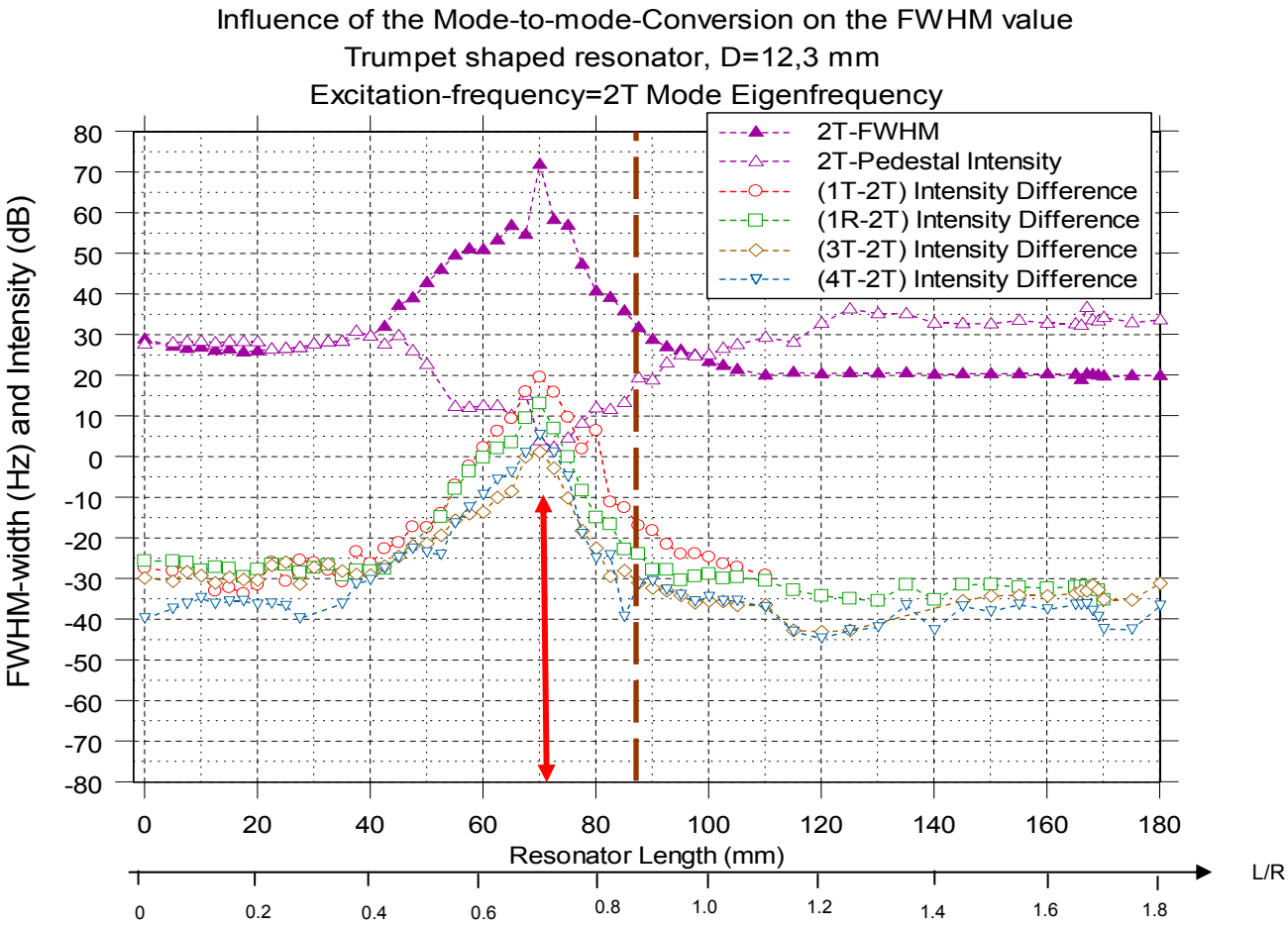

Figure 1.5.6: Mode to mode conversion in a cavity ring coupled with one resonator [5]

The amplitude of the pressure oscillation in the chamber is low and the damping of the eigenmode is high when the frequency of the coupled system is close to one of the resonator eigenfrequencies $f_l = \frac{(2l-1)\cdot c}{4L}$ and far from the cylindrical chamber eigenfrequencies $f_{n,m} = \frac{\alpha_{nm}\cdot c}{2\pi\cdot R}$. In this case energy of the oscillation with the frequency of f_l transforms to oscillations of transverse cylindrical modes with the frequency of $f_{n,m}$. Thus, the oscillation frequency of the coupled system, $f_{osciallation} \approx f_l$, is suppressed but the chamber is not protected from pressure oscillation with the frequency of $f_{n,m}$ as can be seen in figure 1.5.6. For the 2T parental mode this is the case at L/R ≈ 0.71. At this resonator length the measured system frequency crosses the λ/4 hyperbola in figure 1.5.2.

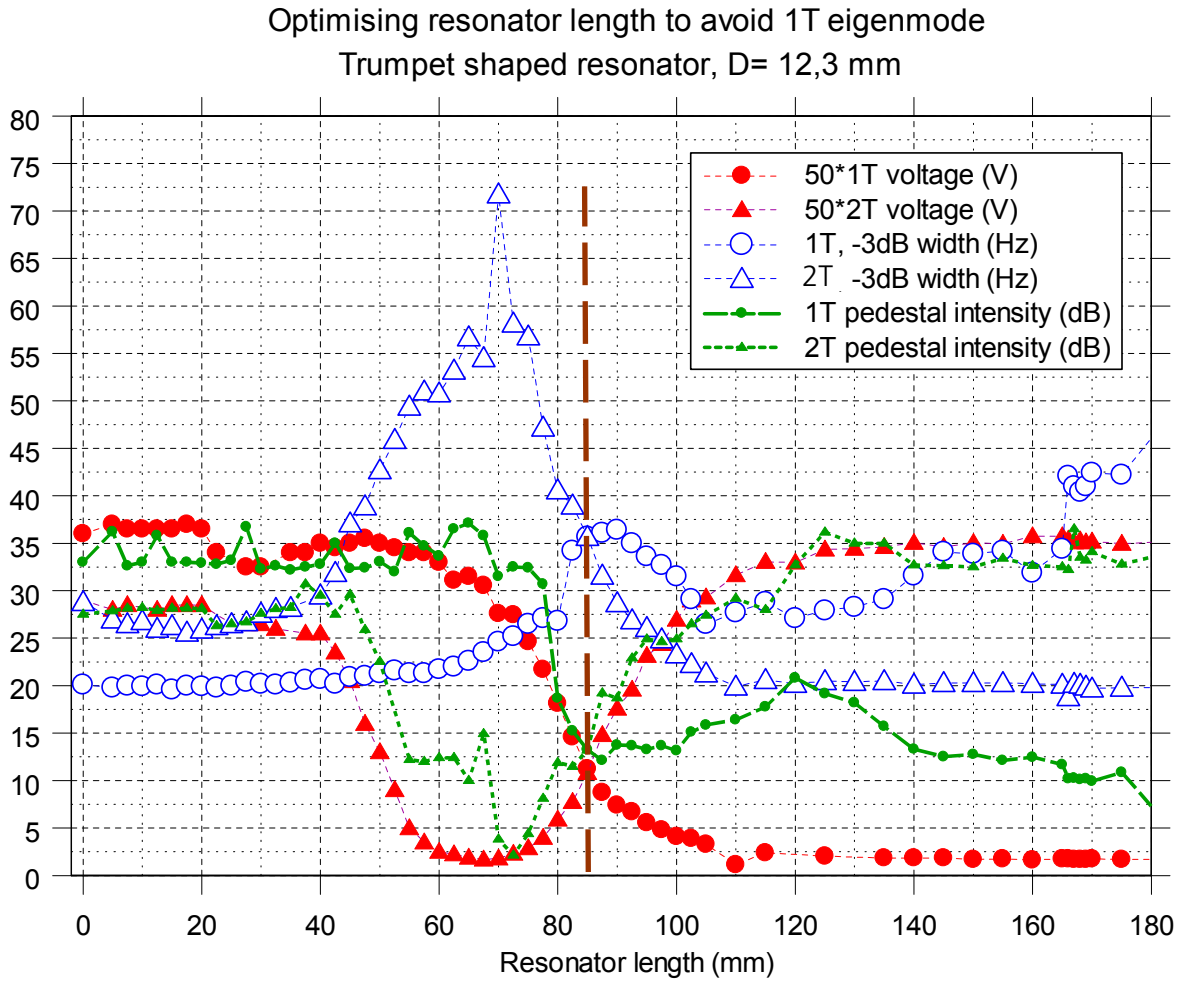

Figure 1.6.1.: Optimal length for damping 1T mode, CRC radius 100 mm [2]

The pressure oscillation is effective suppressed in the chamber for the transverse mode of order *m* and *n* when, for a given constellation of *l*, *m* and *n,* equation (15) is satisfied. In this case the chamber is protected against the pressure oscillation of the acoustical eigenmode satisfying equation (15), but the chamber is not necessarily protected against oscillation of other eigenfrequencies as can be seen in figure 4.1 and table 4.1 [12]. Equation (15) defines the "anti-crossing region" in figure 1.5.2, and the belonging resonator length is called the "optimized resonator length" for protection against the eigenfrequency covered up by equation (15).

Figure 1.6.1 presents the acoustical properties of the modes 1T- and 1T+ for $l=m=n=1$ in equation (15). The anti-crossing for the frequencies is connected with a crossing of all acoustical properties of the concerning modes, thus equation (15) describes an "exceptional point". The special symmetry at this condition leads to a symmetrical frequency distribution as can be seen in figures 3.3.3, 3.4.2, 3.4.3 and 3.4.7. The exceptional point enables to adapt a procedure to adjust acoustical properties of a combustion chamber as described in [10].

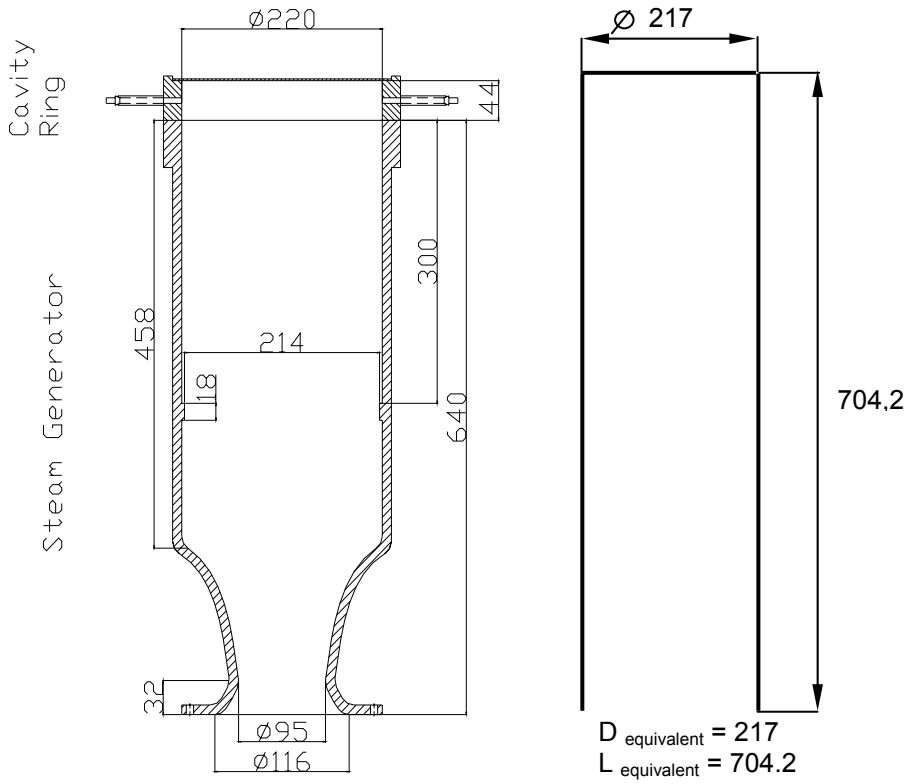

Figure 2.1.1: Geometry of steam generator, and equivalent cylindrical geometry assuming the steam generator being a lambda-quarter tube

The equivalent length to determine the length modes is higher than the geometrical length. It is not the same for the different length modes (see table 3.3.3)!

Figure 2.1.2: SG, test bench

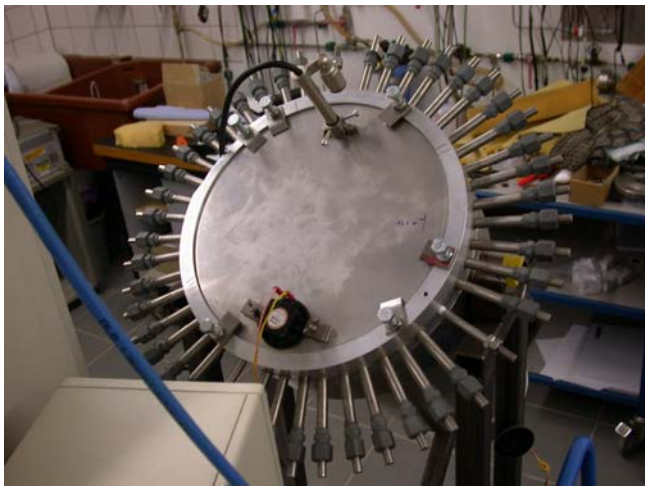

Figure 2.1.3: SG, cavity ring

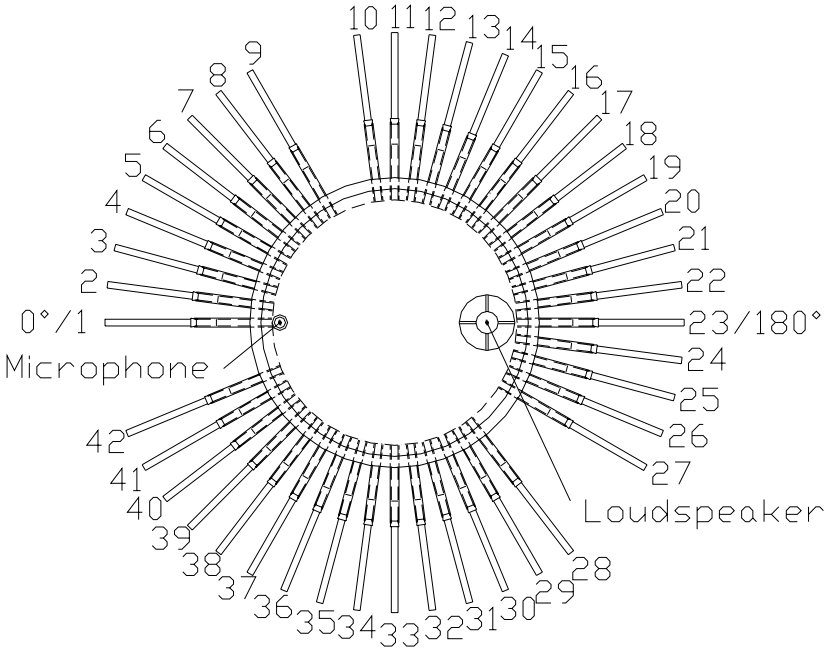

Figure 2.1.4: Geometry of cavity ring

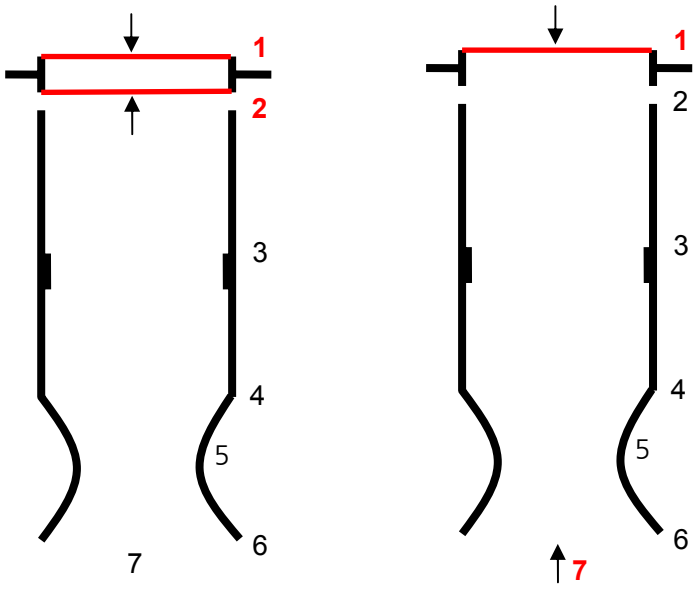

Figure 2.1.5: Scheme of configuration 1-2 and 1-7
Position 1-2: both ends closed
Position 1-7: one end closed, the other end open

	geometric		equivalent	
	Length l_g	**Radius R_g**	**Length l_e**	**Radius R_e**
position 1-2	44 mm	110 mm	44 mm	110 mm
position 1-7	684 mm	110 mm	704,2 mm	108,5 mm

Table 2.1.1: Geometric and equivalent dimensions of the steam generator and cavity ring

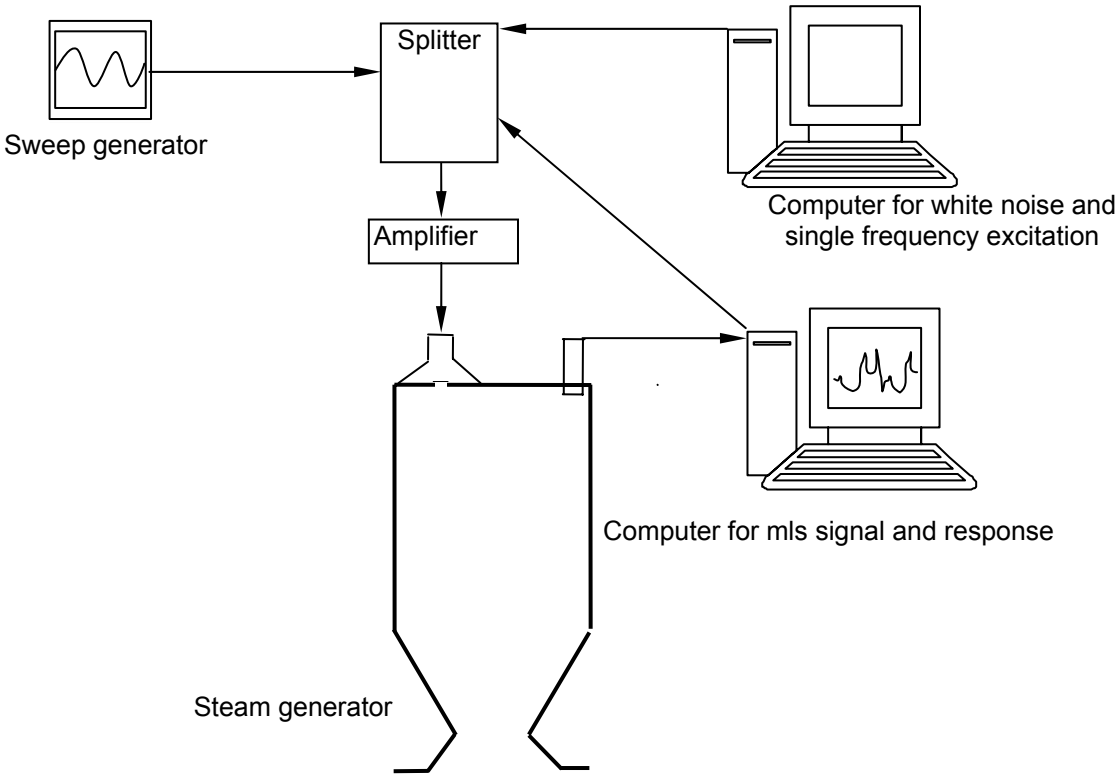

Figure 2.1.7: Scheme of signal flow

	Chapter	Examined task	Description
1	**1.5.**	Influence of resonator length on acoustical properties	position 1-2 (figure 2.1.5), one resonator 0 < L/R < 1.8 Summarization of previous experiments [2 - 5]
2	**3.1.**	Hierarchy of modes	position 1-2 (figure 2.1.5), resonator L/R = 0
3	**3.2.**	Pressure distribution along circumference of cavity ring	position 1-7(figure 2.1.5), 42 resonators, resonator length adjusted for optimal damping of 1T mode (L/R = 0.85), rotation of microphone and speaker in steps of 3,75°
4	**3.3.1.**	Mode-to-mode conversion due to extension of resonator length	position 1-2, 42 resonators, resonator length 0 < L/R < 1, microphone and speaker on metal sheet on top
5	**3.3.2.**		position 1-7, 42 resonators, resonator length 0 < L/R < 1, microphone and speaker on metal sheet on top
6	**3.4.1.**	Optimization of resonator length for chambers with different numbers of resonators	1T mode examined; position 1-2 and 1-7; one and 42 resonators at length for optimal damping of 1T mode (0.81 < L/R < 0.87 compared to L/R = 0)
7	**3.4.2.**		2T mode examined; position 1-2 and 1-7; one and 42 resonators at length for optimal damping of 2T mode (L/R = 0.49 compared to L/R = 0)

Table 3.1: Overview of enforced test series

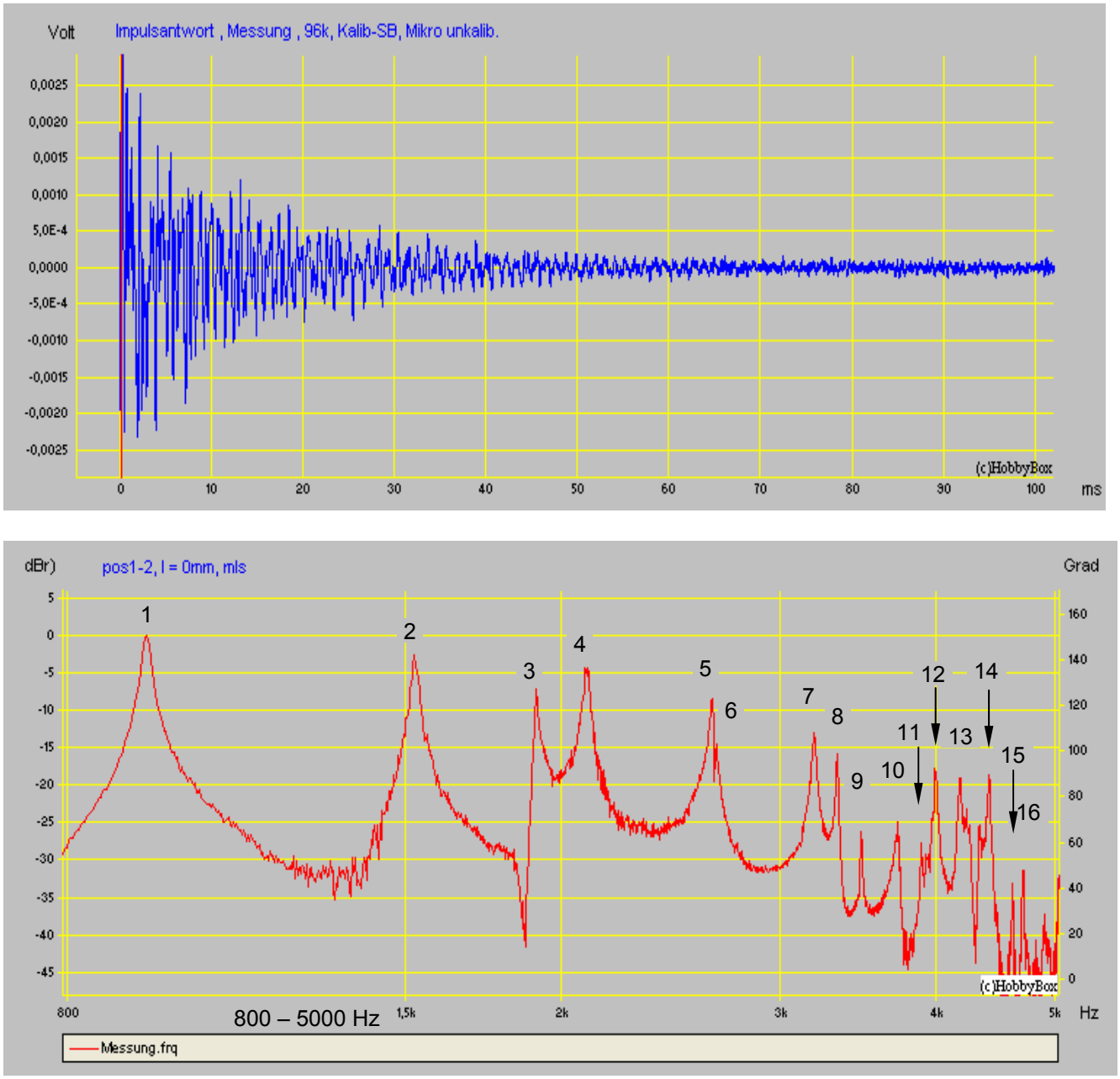

Figure 3.1.1: Pulse response and frequency distribution after MLS excitation, position 1-2, mode identification: table 3.1.1

No.	n	m	α_{nm}	Mode	Calculated frequency (Hz)	Measured frequency (Hz)	Relative energy density Imax = 100%	Spectral energy density Σ =100 %
1	1	1	1.8410	1T	919	930	100	41.6
2	2	1	3.0541	2T	1525	1530	50	20.8
3	0	2	3.8318	1R	1913	1910	20	8.3
4	3	1	4.2013	3T	2097	2100	40	16.6
5	4	1	5.3175	4T	2654	2660	16	6.7
6	1	2	5.3320	1R1T	2661	2670	4.5	1.7
7	5	1	6.4160	5T	3203	3210	5	2.1
8	2	2	6.7085	1R2T	3349	3350	2.5	0.9
9	0	3	7.0155	2R	3502	3500	0.25	<0.1
10	6	1	7.5018	6T	3745	3740	0.3	0.1
11	-	-	-	1L	3920	3910	0.1	<0.1
-	3	2	8.0146	1R3T	4001	not found	-	-
12	-	-	-	1L1T	4026	4010	1.6	0.4
13	-	-	-	1L2T	4206	4200	1.3	0.25
-	1	3	8.5363	2R1T	4261	very weak	-	-
-	7	1	8.5781	7T	4282	not found	-	-
-	-	-	-	1L1R	4362	very weak	-	-
14	-	-	-	1L3T	4446	4430	1.3	0.25
15	4	2	9.2825	1R4T	4634	4620	<0.1	<0.1
16			-	1L4T	4734	4720	<0.1	<0.1
17	8	1	9.6475	8T	4816	4820	<0.1	<0.1

Table 3.1.1: The first 17 identified modes according figure 3.1.1. [2]

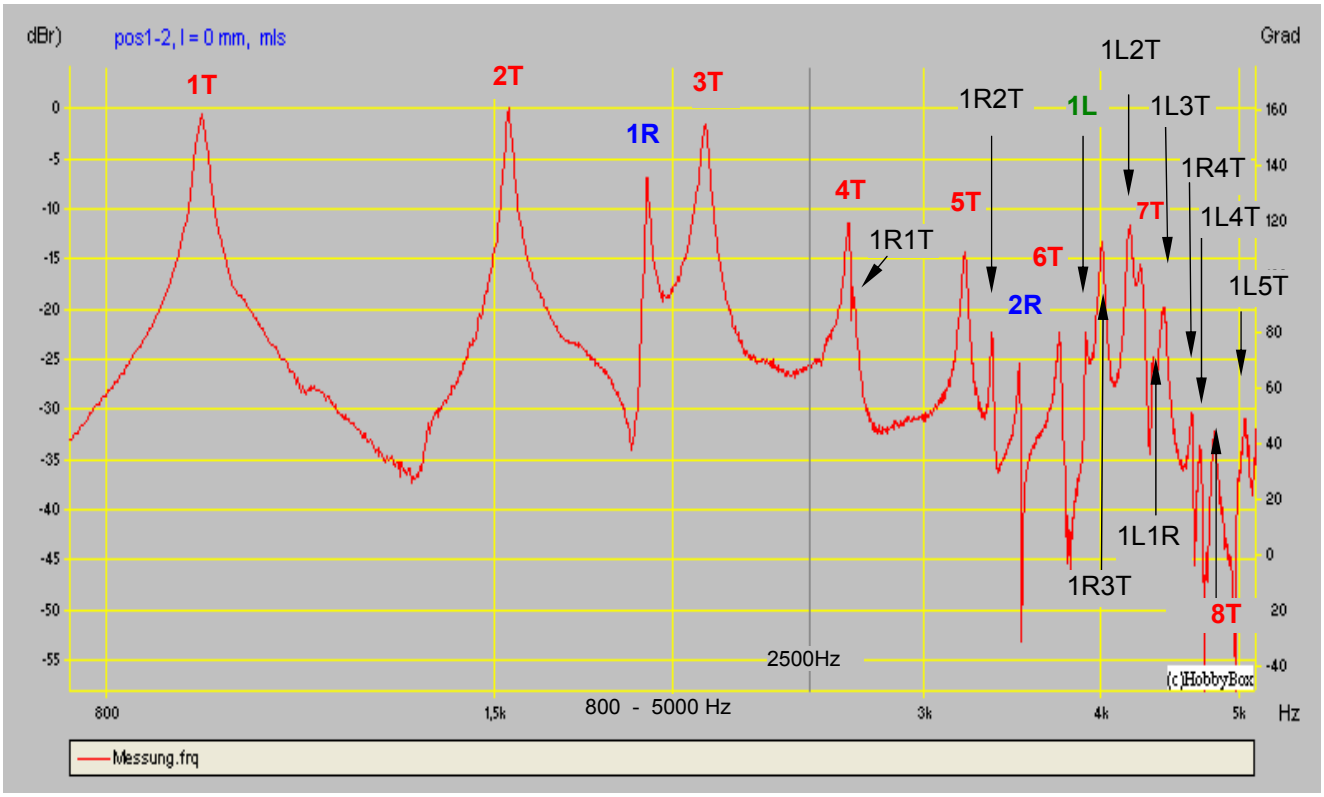

Figure 3.3.1: Overview of modes, position 1-2, resonator length 0 mm

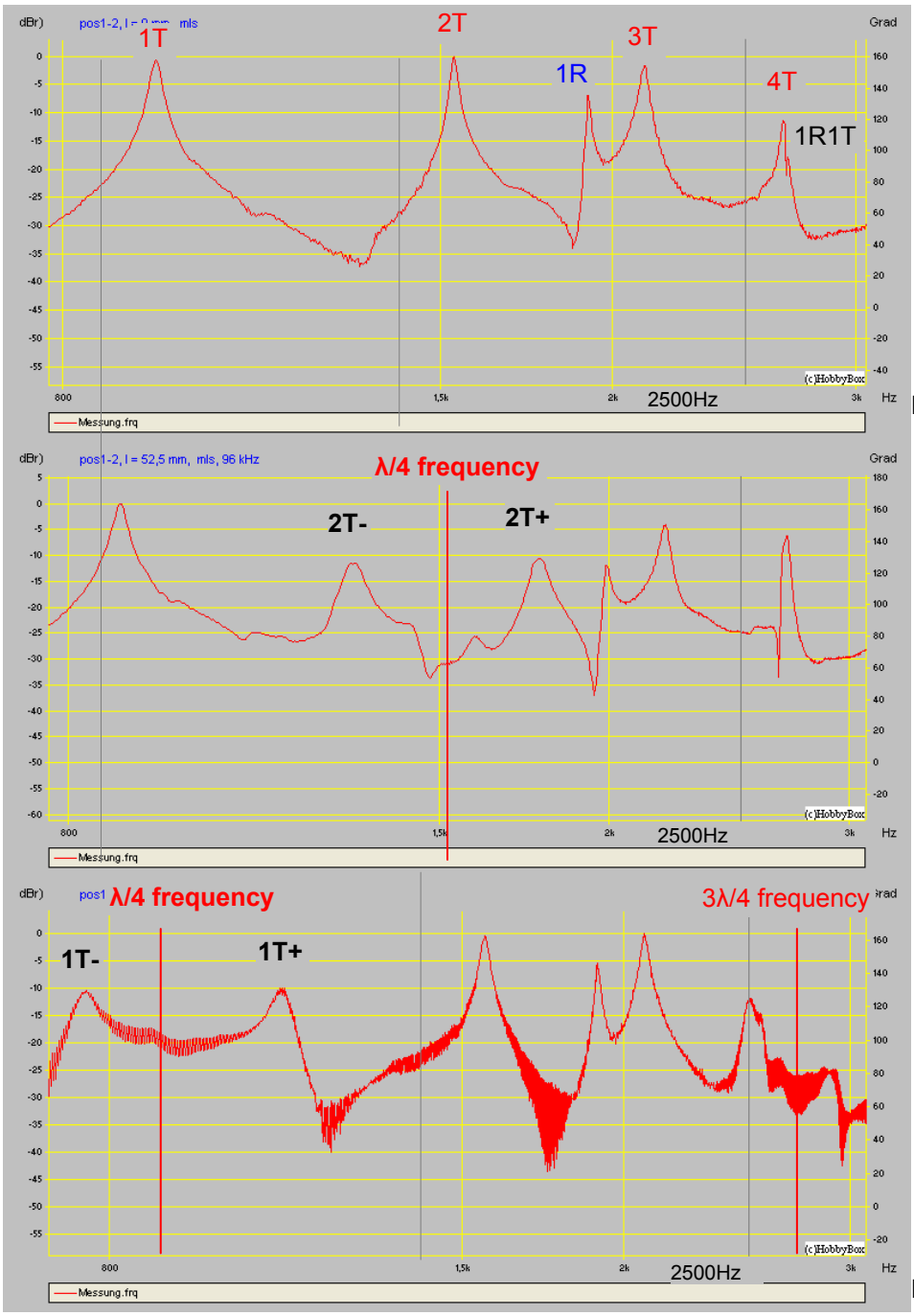

Figure 3.3.3: Frequency distribution between 800 and 3000 Hz, *L/R* = 0/ 0.477/ 0.818 , position 1-2, 42 resonators

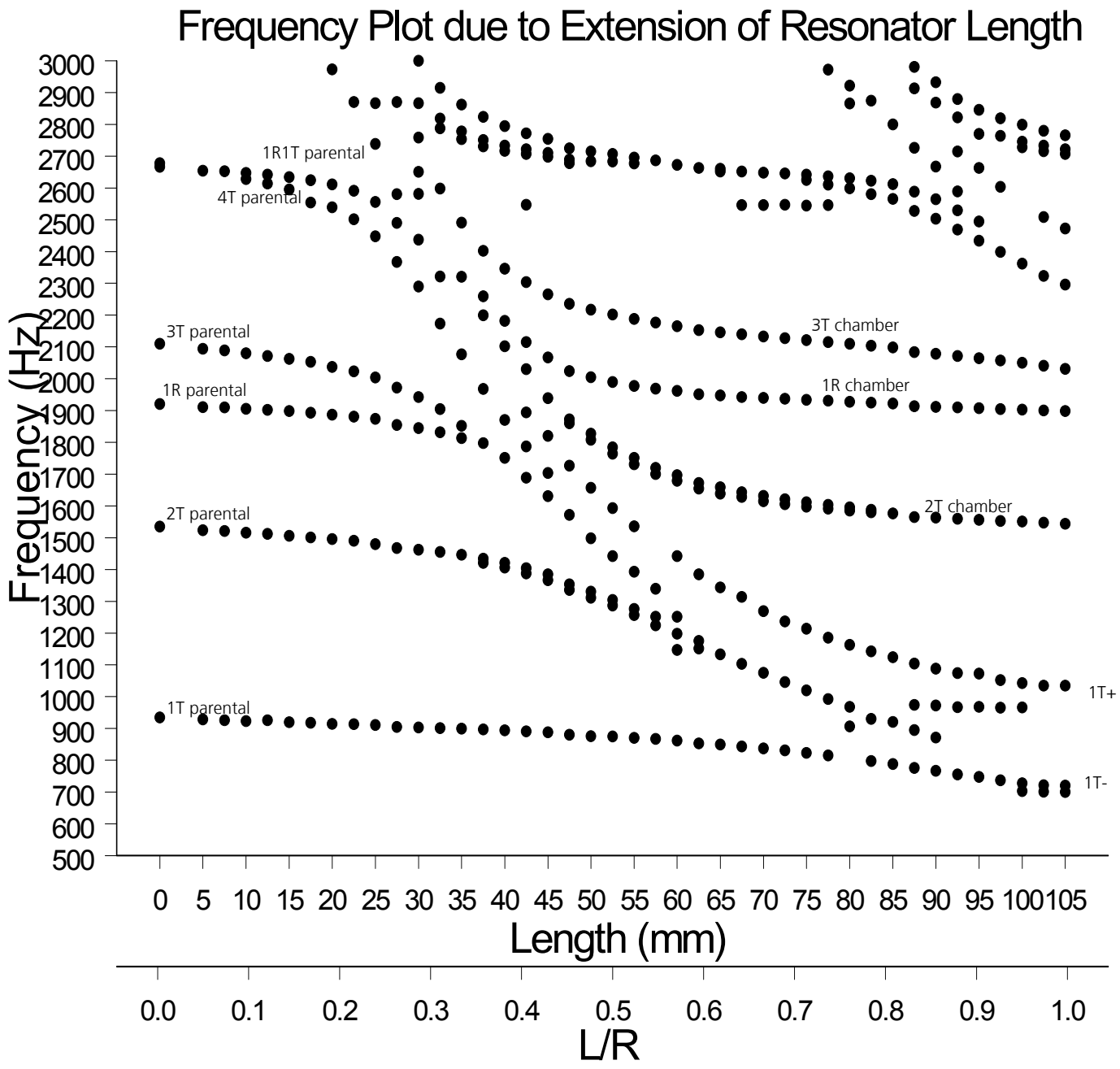

Figure 3.3.4: Measured course of the modes for position 1-2, 42 resonators

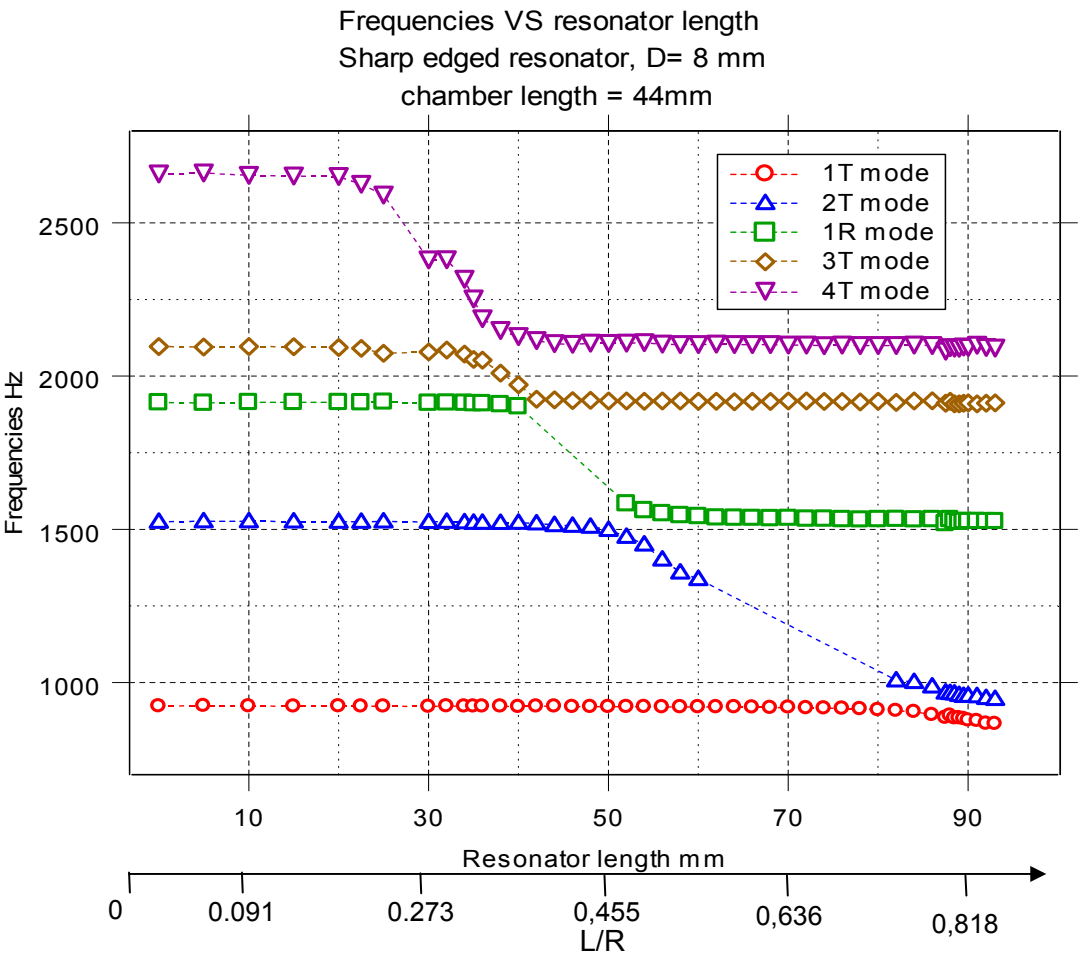

Figure 3.3.5: Measured course of the modes for one resonator, position 1-2, [6]

	$f_{L=0}$ (Hz)	$f_{equation\ (15)}$ (Hz)	$L/R_{equation\ (15)}$
1T	935	not found	1,663
2T	1535	not found	1,013
1R	1920	1913	0,81
3T	2110	2110	0,737
4T/ 1R1T	2666	2663	0,583

Table 3.3.1: Mode frequencies for parental modes at *L/R* = 0 and cylindrical chamber modes near to solve equation (15)

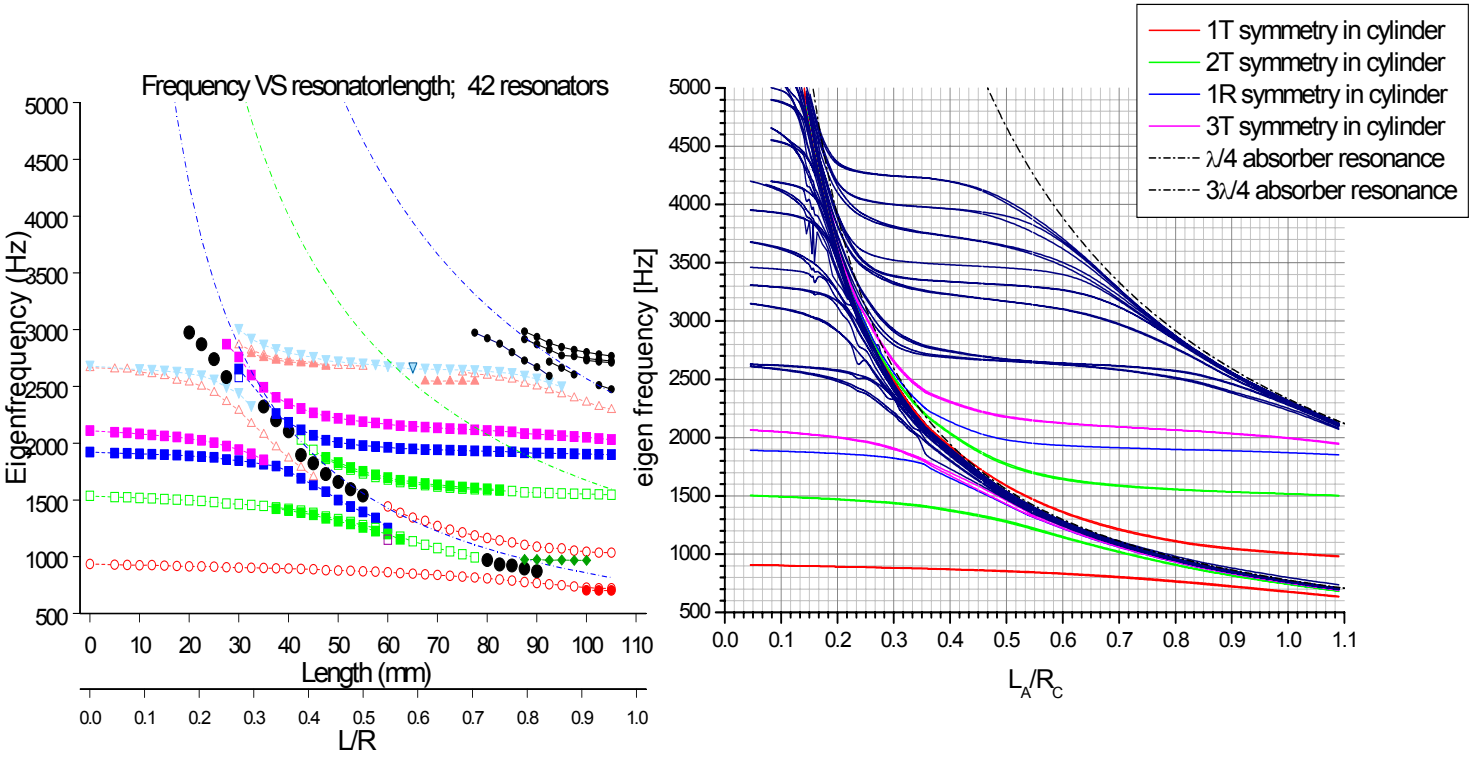

Figure 3.3.6: Classification of modes according to calculation of FlexPDE [8], measurement compared with calculus, position 1-2, [2]

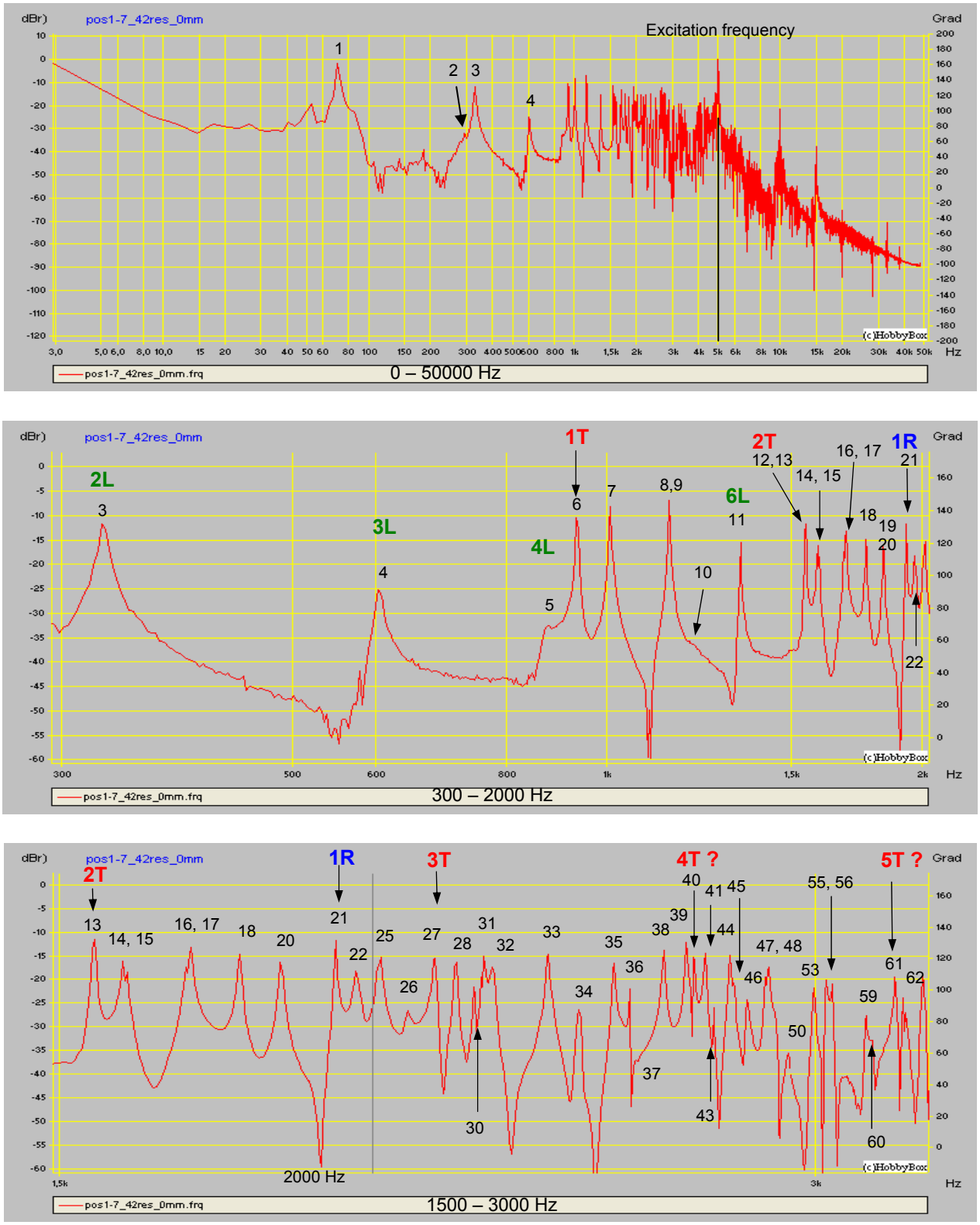

Figure 3.3.11: Acoustical modes, *L*/*R* = 0, position 1-7, (mode identification: Table 3.3.2)

No.	Mode	5000 Hz excitation			calculated frequency	single frequency				
		f (Hz)	w (Hz)	PI (dB)		f (Hz)	w (Hz)	PI (dB)	U (V)	E (%)
1	Helmholtz? 1L?	85	5,9	22	78 122.2	85	7,4	32	0,068	99,5
2	Speaker	291	12,6	2	-					
3	2L	328,1	4,3	25	366,6	328,1	4,2	38	0,24	99,93
4	3L	600,6	2,2	19	611	600,7	7,2	35	0,1	97,31
5	4L	864,2	21	4	855,4	870,2	18,7	9	0,036	6,54
6	1T	931,7	4,4	27	929,17	934,6	4,2	30	0,256	99,52
7	2L1T	1002	3	21	998,78	1004,9	2,3	29	0,252	98,33
8	5L				1099,8	1092,7	23,8	2	0,04	0,36
9	3L1T	1139,6	2,4	22	1111,83	1142,6	3,4	37	0,26	99,82
10	4L1T				1262,57	1253,3	20	32	0,02	0,09
11	6L	1333	2,9	31	1344,2	1338,8	2,9	39	0,18	99,54
12		1532,2	4,6	8		1538,1	8,8	2	0,16	16,5
13	2T	1538,1	6,8	2	1541,41	1546,9	4,4	11	0,12	93,33
14	2L2T	1587,8	6,3	20	1584,35	1587,8	3,4	5	0,2	49,14
15	7L				1588,6	1593,7	3,3	6	0,19	58,46
16	6L1T	1675,8	?	?	1633,33	1684,5	12,6	1	0,24	32,87
17	3L2T	1681,5	6,5	2	1657,95	1690,4	4,1	5	0,26	74,9
18	4L2T	1760,6	5,3	8	1762,58	1766,9	6,2	23	0,16	95,12
19	8L	1825,2	5,3	2	1833	1834	5,4	3	0,284	5,13
20	7L1T	1831	3,4	5	1839,45	1839,9	3,4	6	0,316	70,53
21	1R	1921,9	1,9	17	1924,84	1930,7	1,8	28	0,11	98,87
22	2L1R	1960,1	?	?	1959,39	1968,8	6,9	3	0,13	36,81

Table 3.3.2: Acoustical modes for L/R = 0, position 1-7, transversal modes highlighted

$$L_{equivalent}\ (l) \equiv L_l = \frac{(2 \cdot l - 1) \cdot c}{4 \cdot f_l} \tag{16}$$

$$D_{l,n} = \frac{f_l \cdot (2 \cdot (l+n) - 1)}{f_{l+n} \cdot (2 \cdot l - 1)} - 1 \tag{17}$$

Order of mode	Mode	Measured frequency	Equivalent length of the SG	Deviation from the harmonic and convergence of the equivalent length VERSUS l and n		
l		f_l	L_l (eq.(16))	n	$D_{l,n}$ (eq.(17))	$\frac{L_l}{L_{l+n}} - 1$
-	-	Hz	m	-	-	-
1	1L	85	1.01206	1	-0.22279793	0,28666667
2	2L	328.1	0.79875	1	-0.08967316	0,09850655
3	3L	600.7	0.71604	1	-0.03357849	0,03474518
4	4L	870.2	0.69200	1	0.02391194	-0,02335351
5	5L	1092.7	0.70854	1	-0.0024483	0,0024543
6	6L	1338.8	0.70681	1	-0.0072045	0,00725679
7	7L	1593.7	0.70172	1	0.00266337	-0,00265629
8	8L	1834	0.703585	1	0.00772488	-0,00766566
9	9L	2062.6	0.709020	2	-0.00120829	0,00120975
10	10L	not found	--		--	--
11	11L	2551	0.708163	2	0.0015516	-0,0015492
12	12L	not found	--		--	--
13	13L	3032.2	0.709262	-4	-0.0003413	0,00034167

Table 3.3.3: Frequencies, equivalent lengths and deviation from the harmonic for the length modes of the steam generator

For the equivalent length see figure 2.1.1.
The length mode overtones are non-harmonic! $D_{l,n}$ is the deviation of the harmonic.

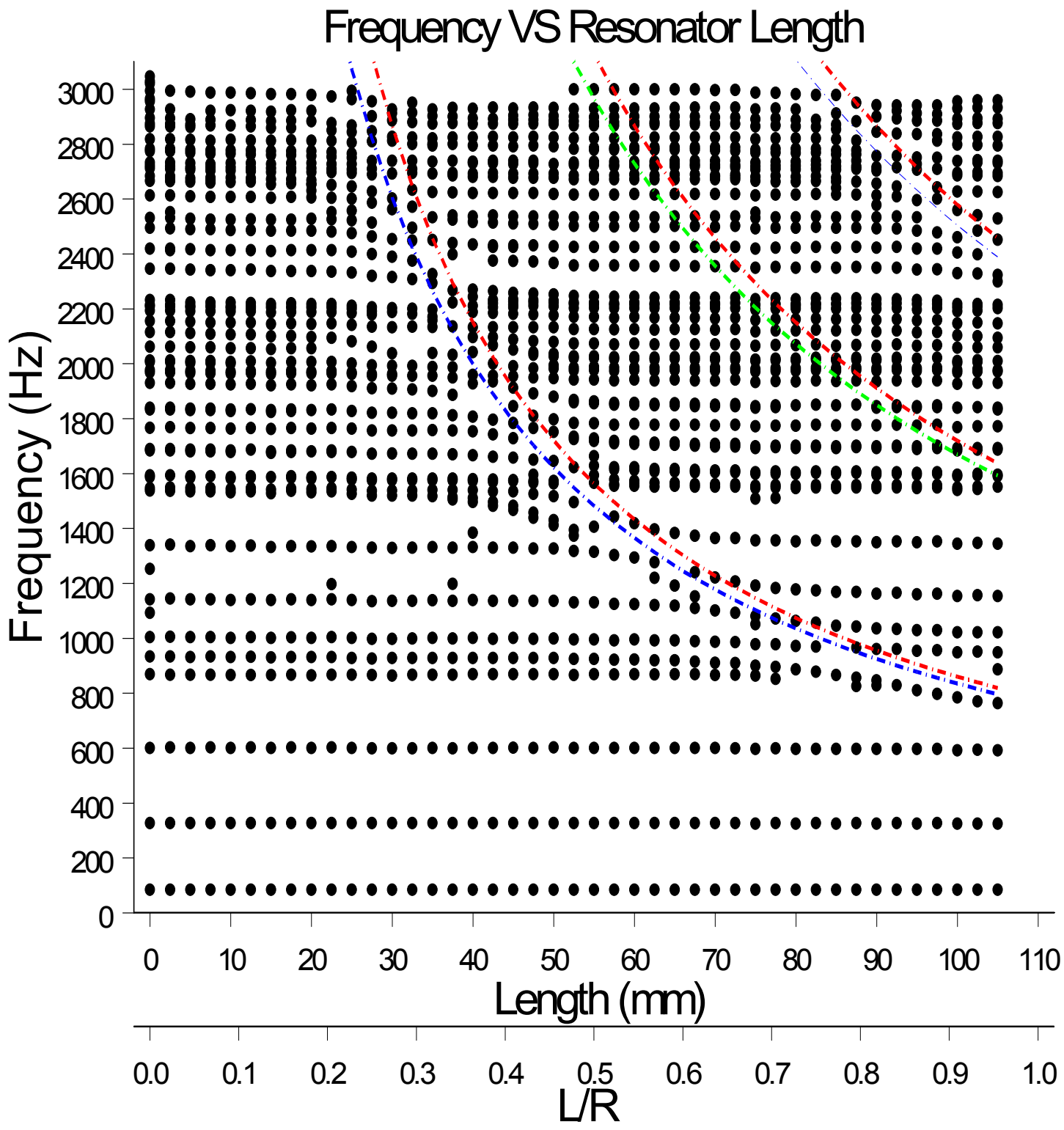

Figure 3.3.16: Measured curse of modes, position 1-7, 42 resonators

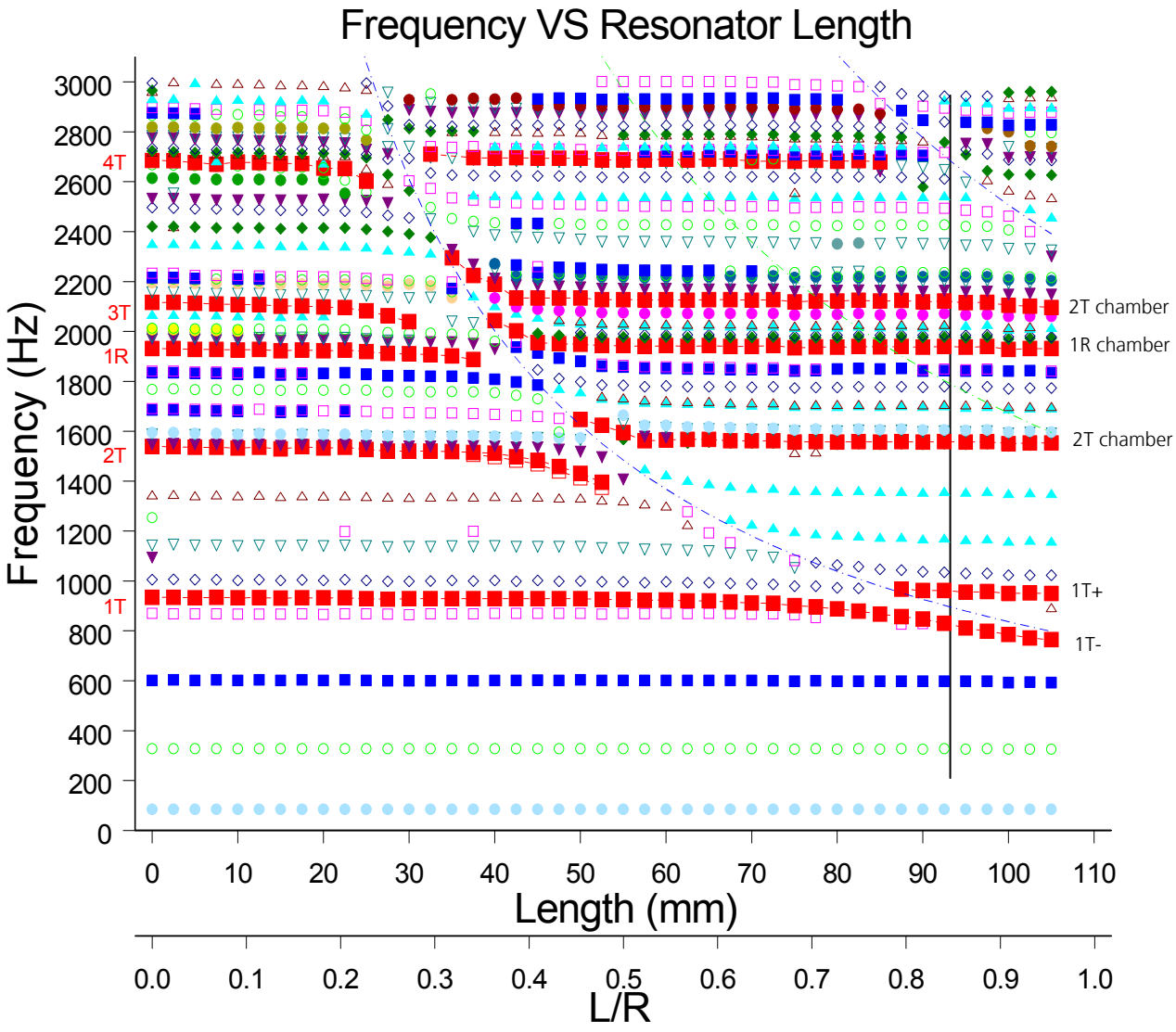

Figure 3.3.17: Classification of modes, transverse modes highlighted

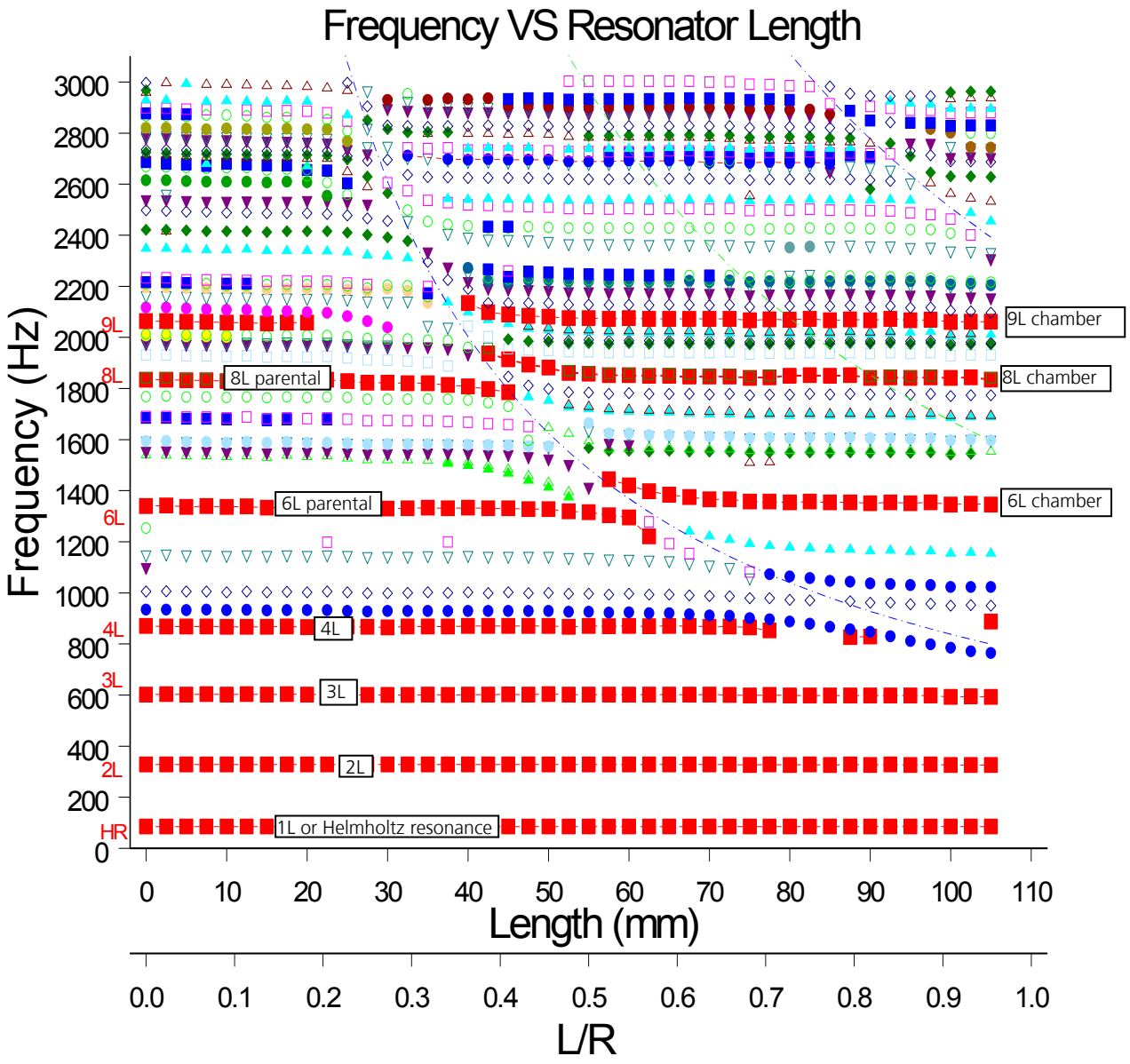

Figure 3.3.18: Classification of modes, length modes highlighted

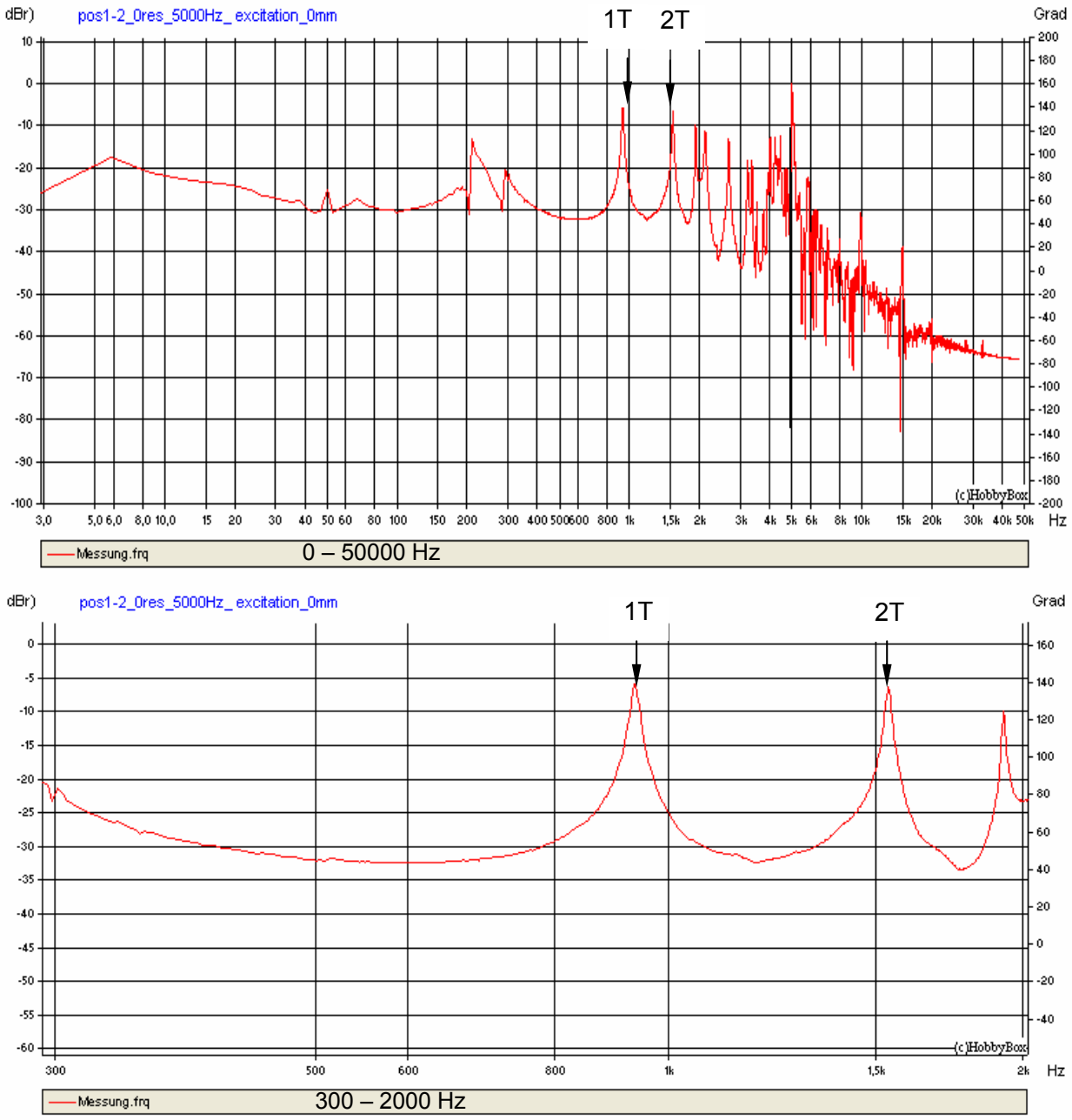

Figure 3.4.1: Frequency response, position 1-2, resonator length 0 mm, 5000 Hz excitation

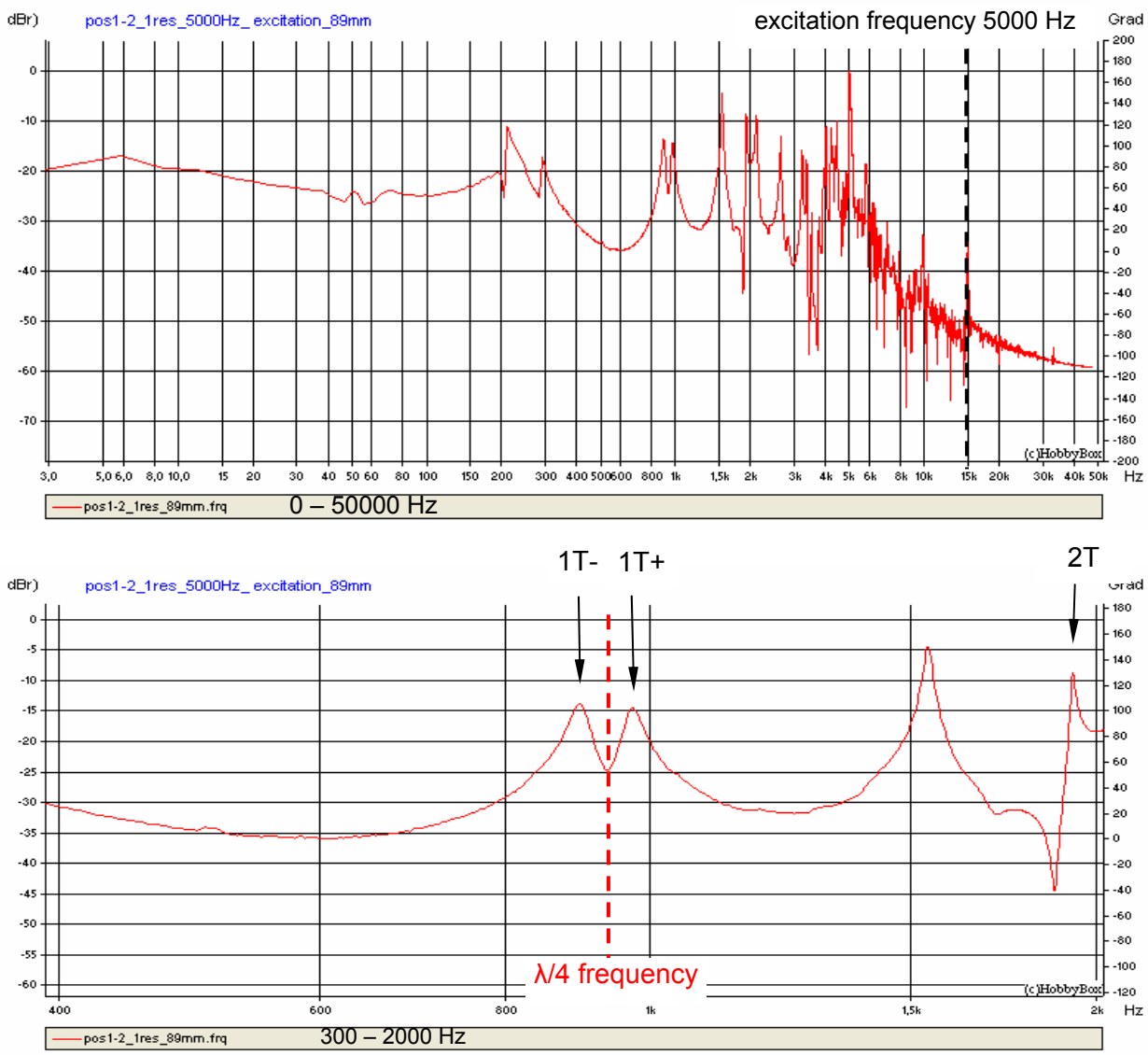

Figure 3.4.2: Frequency response, position 1-2, one resonator *at* L/R = 0,809

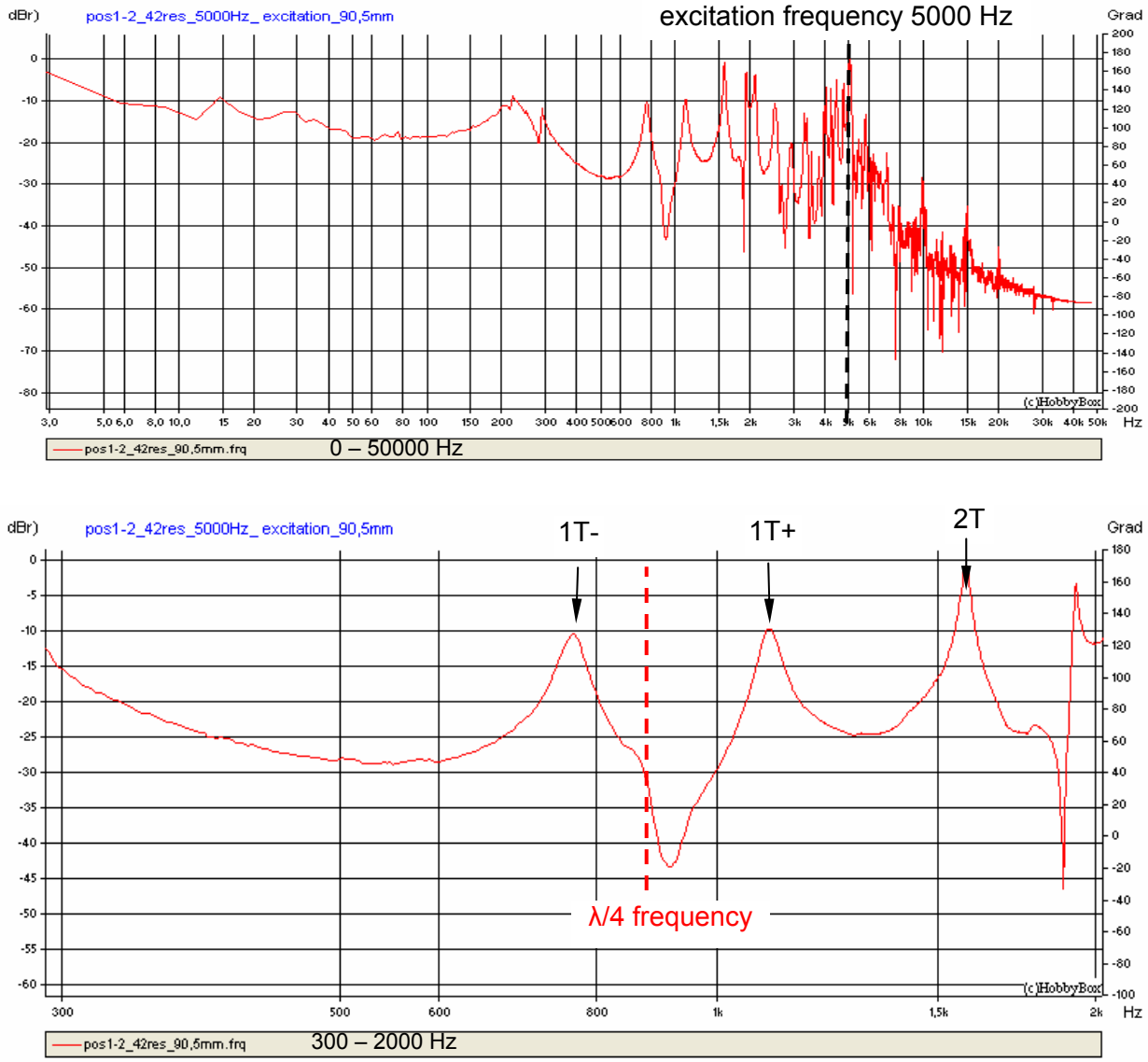

Figure 3.4.3: Frequency response, position 1-2, 42 resonators, *L*/*R* = 0,823

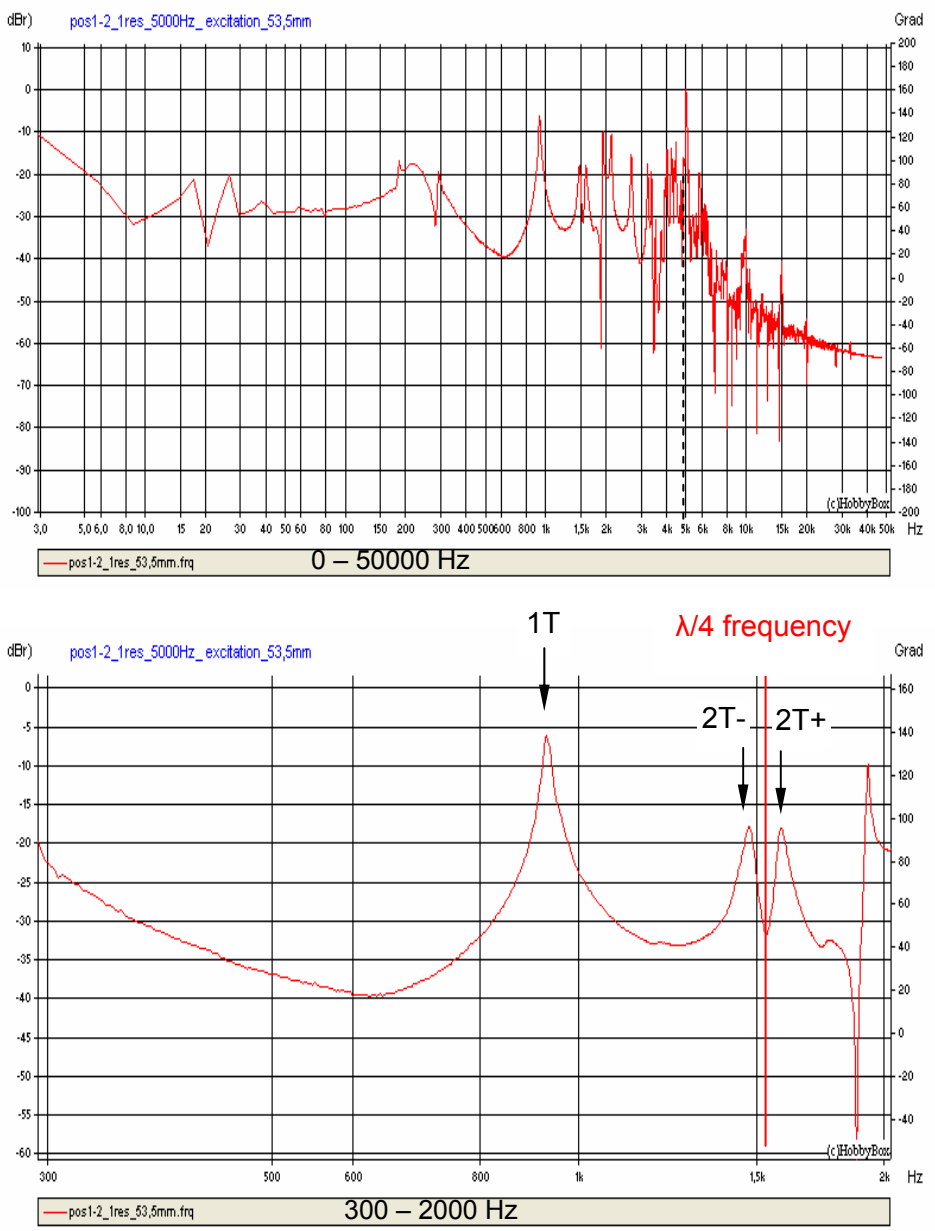

Figure 3.4.7: Frequency response, position 1-2, one resonator, *L*/*R* = 0,49

2 Conclusion

In this study acoustical experiments on a laboratory scale combustion chamber and a steam generator are presented. The acoustical properties of the steam generator are modified by a varying number of damping elements. For the excitation of the oscillations different signals are used. The acoustic attributes are derived from the FFT analysis of the decaying signal.

The cylindrical chamber has a radius of 110 mm and a length of 44 mm. 42 resonators (lambda-quarter tubes) are inserted to the chamber to control its acoustical properties. The resonator diameter is 9 mm, the length was varied in the range of 0 < L/R < 1 with L/R as the ratio of the resonator length to the chamber radius. While varying the length of one resonator the length of the other 41ones was kept constant at L/R = 0. In the experiments with 42 resonators the lengths of all resonators did have the same value.

Experiments with short cylindrical chamber without resonator

Experiments with the short chamber and without acoustic elements, i.e. resonator length of L/R = 0, show a clear hierarchy of acoustic modes: Energy of high frequency oscillation converts to acoustical modes with lower eigenfrequencies. The most stable acoustical mode is the first tangential one followed by the 2T and 3T modes (Chapter 3.1).

Experiments with short cylindrical chamber coupled to one resonator

Summary of previous experiments [3 - 5] using short cylindrical chamber coupled to one resonator is presented in chapter 1.5. Frequency and damping of the acoustical modes are shown in figure 1.5.2. With increasing resonator length the frequency of the coupled system continuously decreases. The coupled frequency of the chamber-resonator-system converges either to one of the eigenfrequencies of the chamber without resonator or to one of the eigenfrequencies of the resonator without cylindrical chamber.

The amplitude of the pressure oscillation is high and the damping of the eigenmode is low when the frequency of the coupled system is close to one of the eigenfrequencies of the chamber. This is the case when the resonator length is zero or when, for a given resonator length and a given constellation of *l*, *m* and *n*, the equation (14) $l \cdot \frac{c}{2L} = \frac{\alpha_{n,m} \cdot c}{2 \cdot \pi \cdot R}$ is satisfied.

The amplitude of the pressure oscillation in the chamber is low and the damping of the eigenmode is high when the frequency of the coupled system is close to one of the resonator eigenfrequencies $f_l = \frac{(2l-1) \cdot c}{4L}$ and far from the cylindrical chamber eigenfrequencies $f_{n,m} = \frac{\alpha_{nm} \cdot c}{2\pi \cdot R}$. In this case energy of the oscillation with the frequency of f_l transforms to oscillations of transverse cylindrical modes with the frequency of $f_{n,m}$. Thus, the oscillation frequency of the coupled system, $f_{osciallation} \approx f_l$, is suppressed but the chamber is not protected from pressure oscillation with the frequency of $f_{n,m}$ as can be seen in figure 1.5.6.

The pressure oscillation is effective suppressed in the chamber for the transverse mode of order *m* and *n* when, for a given constellation of *l*, *m* and *n,* equation (15) $\frac{(2 \cdot l - 1) \cdot c}{4 \cdot L} = \frac{\alpha_{n,m} \cdot c}{2 \cdot \pi \cdot R}$ is satisfied. In this case the chamber is protected against the pressure oscillation of the acoustical eigenmode satisfying equation (15), but the chamber is not necessarily protected against oscillation of other eigenfrequencies as can be seen in figure 4.1 and table 4.1 [12]. Equation (15) defines the "anti-crossing region" in figure 1.5.2, and the belonging resonator length is called the "optimized resonator length" for protection against the eigenfrequency covered up by equation (15). Table 3.1.1 contains values for $1.8 < \alpha_{n,m} < 10$.

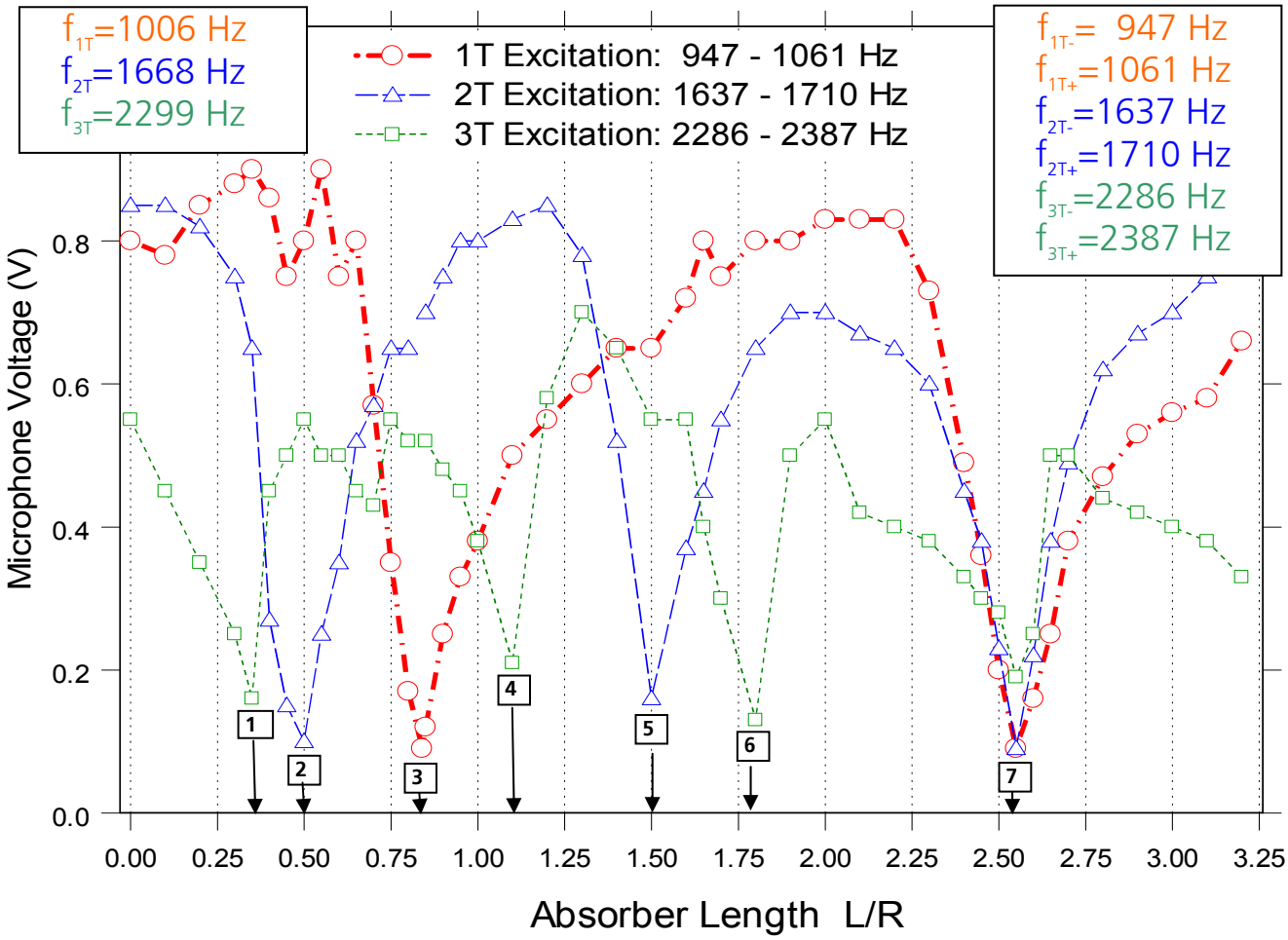

Figure 4.1: Microphone signal VERSUS resonator length for a cylindrical chamber coupled with one resonator [12]; excitation with sweeping frequencies in the ranges of $f_{1T-} - f_{1T+}$, $f_{2T-} - f_{2T+}$ and $f_{3T-} - f_{3T+}$

optimized length No.	1	2	3	4	5	6	7
L/R experiment	0.35	0.50	0.84	1.10	1.50	1.80	2.55
L/R equation (15)	0.37	0.52	0.85	1.11	1.54	1.87	2.52, 2.57, 2.59
l	1	1	1	2	2	3	2, 2, 2
m	1	1	1	1	1	1	1, 1, 1
n	3	2	1	3	2	3	1, 2, 3
suppressed mode	3T	2T	1T	3T	2T	3T	1T, 2T, 3T
non-suppressed mode	2T,1T	3T,1T	2T,3T	2T,1T	1T,3T	1T,2T	- - -

Table 4.1: Optimized resonator length to suppress the first three tangential modes using the basic tone, the first and second overtones of the resonator for suppressing pressure oscillation

Experiments with short cylindrical chamber coupled to 42 resonators

In chapters 3.2, 3.3.1 and 3.4, experiments on short cylindrical chamber with a cavity ring are described. The cavity ring contains 42 resonators (figures 2.1.3 and 2.1.4). Comparing figures 1.5.2, 3.3.5 and 3.3.6 we can observe the difference in the frequency change as a function of the cavity length: For one cavity, the frequency converges from the level of $f_{n,m}$ to the neighboring lower level according the ranking of $\alpha_{n,m}$ (table 3.1.1) with increasing cavity length when the frequencies $f_{n,m}$ (equation (8)) and f_l (equation (7)) should cross, however, they show an avoided crossing. For 42 cavities, the frequency converges from $f_{n,m} = \frac{\alpha_{nm} \cdot c}{2\pi \cdot R}$ to $f_l = \frac{(2l-1) \cdot c}{4L}$.

The effect of the cavity ring is higher than that of one cavity due to the higher affecting area for the multiplicity of cavities. Consequently, the measurements with the cavity ring are more difficult than those with one cavity. This leads to higher signal-to-noise ratio and to a higher measuring error especially for the measurements of the line width.

Nevertheless, there are two similarities between the effects of one resonator and a cavity ring: First: The amplitude of the pressure oscillation is high and the damping of the eigenmode is low when the frequency of the coupled system is close to one of the eigenfrequencies of the chamber. This is the case when the resonator length is zero or when, for a given resonator length, the equation (14) $l \cdot \frac{c}{2L} = \frac{\alpha_{n,m} \cdot c}{2 \cdot \pi \cdot R}$ is satisfied for a given constellation of *l*, *m* and *n*. Second: There is no pressure oscillation in the chamber for the transverse mode of order *m* and *n* when for a given constellation of *l*, *m* and *n* if equation (15) $\frac{(2 \cdot l - 1) \cdot c}{4 \cdot L} = \frac{\alpha_{n,m} \cdot c}{2 \cdot \pi \cdot R}$ is satisfied. Consequently, the optimized resonator length is the same for a cylindrical chamber with one cavity and for a chamber coupled to a cavity ring.

Experiments regarding the length of the combustion chamber

Figures 2.1.1 and 2.1.5 and table 2.1.1 contain the sketches and dimensions for the concerning experiments. Previous investigations [6] taught that for cylindrical chambers the damping of the acoustical modes is reversed proportional to the cylinder length. Thus, for very short cylinders the increase of the length increases the accuracy of the measurement, too, while further increasing the chamber length the frequencies of the length modes overlap the frequencies of the lower order transverse ones. The consequence is an enormous growth of measuring difficulties. This can be easily understood comparing the figures 1.5.2 (short chamber, one cavity), 3.3.4 (short chamber, cavity ring) and 3.3.16 (long chamber, cavity ring). The multiplicity of the modes hinders the correct measurement of the FWHM. A further difficulty for real engine geometry is the nozzle at the chamber exit leading to a reduced chamber radius at the end of the chamber. This leads to falsified eigenfrequencies of the length modes compared to ideal cylinder geometry as presented in table 3.3.3, and prevents the correct mode identification. Nevertheless, it can be stated that eigenmodes satisfying equation (14) $l \cdot \frac{c}{2L} = \frac{\alpha_{n,m} \cdot c}{2 \cdot \pi \cdot R}$ are not damped, and eigenmodes satisfying equation (15) $\frac{(2 \cdot l - 1) \cdot c}{4 \cdot L} = \frac{\alpha_{n,m} \cdot c}{2 \cdot \pi \cdot R}$ are suppressed by the cavity ring.

3 Bibliographical reference

[1] B. Knapp, M. Oschwald, S. Anders: Untersuchung der tangentialen Moden von hochfrequenten Verbrennungsinstabilitäten in Raketenbrennkammern; DGLR – Jahrestagung 2005, Paper No. 189, September 2005

[2] Z. Faragó, M. Oschwald: Resonance Frequencies and Damping in Combustion Chambers with Quarter Wave Cavities; 6th Symposium on Launcher Technologies, November 8th to11th, 2005, Munich

[3] McEniry, Z. Faragó: Study into the damping characteristics of the CRC coupled with Acoustic Elements; E. DLR-LA-HF-RP-007

[4] A. Uryu, Z. Faragó: Investigation on the Damping Behaviour of the CRC combined with Acoustic Elements; DLR-LA-HF-RP-009

[5] T. Barbotin, Z. Faragó: Study on Acoustic Resonators coupled to a Combustion Research chamber;

[6] G. Dellea, Z. Faragó: Study into the Damping Characteristics of a Steam Generator coupled with acoustic Elements;

[7] Lawrence E. Kinsley: Fundamentals of Acoustics; John Wiley & Sons

[8] M. Oschwald: Numerical Determination of Eigenfrequencies and Admittances for Multi Cavity Resonator Configurations; DLR-LA-HF-RP-018

[9] G. Searby and F. Cheuret: Laboratory scale investigations of acoustic instability in a cylindrical combustion chamber, Proceedings of 7th French-German Colloquium on Research in Liquid Rocket Propulsion, 17-18 September 2002, Orléans France. CDROM,
Editors I. Gökalp and C. Chauveau, LCSR Orléans.

[10] Z. Faragó: Procedure to adjust acoustical properties of a combustion chamber; Patent application, German Patent Office, German Aerospace Establishment ; Application No. 10 2005 035 085.2, July 2005

[11] G. Krühsel and K. Schäfer: Design and Development of an Ethanol/LOX Injection Head for Rocket Steam Generator (45 kg/s Steam) and Experimental Study of Combustion Stability; Fourth International Conference on Green Propellants for Space Propulsion, 20-22 June 2001, EXTEC, Noordwijk, NL

[12] Z. Faragó: Acoustical damping of a combustion chamber;
Patent application, German Patent Office, German Aerospace Establishment ;
Application No. 10 2006 007 711.3, February 2006